A new estimation of equivalent matrix block sizes in fractured media with two-phase flow applications in dual porosity models

Chahir Jerbi, André Fourno, Benoit Noetinger, Frédérick Delay

▶ **To cite this version:**

Chahir Jerbi, André Fourno, Benoit Noetinger, Frédérick Delay. A new estimation of equivalent matrix block sizes in fractured media with two-phase flow applications in dual porosity models. Journal of Hydrology, 2017, 548, pp.508-523. 10.1016/j.jhydrol.2017.03.028 . hal-01738345

HAL Id: hal-01738345
https://ifp.hal.science/hal-01738345

Submitted on 20 Mar 2018

HAL is a multi-disciplinary open access archive for the deposit and dissemination of scientific research documents, whether they are published or not. The documents may come from teaching and research institutions in France or abroad, or from public or private research centers.

L'archive ouverte pluridisciplinaire **HAL**, est destinée au dépôt et à la diffusion de documents scientifiques de niveau recherche, publiés ou non, émanant des établissements d'enseignement et de recherche français ou étrangers, des laboratoires publics ou privés.

A new estimation of equivalent matrix block sizes in fractured media with two-phase flow applications in dual porosity models

Chahir Jerbi[1], André Fourno[1], Benoit Noetinger[1], Frederick Delay[2 *]

[1] IFP Energies Nouvelles, 1&4 Avenue du Bois Préau 92500 Rueil-Malmaison, France.

[2] Laboratoire d'Hydrologie et de Géochimie de Strasbourg, Univ. Strasbourg/EOST, CNRS UMR 7517, 1 rue Blessig, 67000 Strasbourg, France

* Corresponding author: Phone +33 3 68 85 04 16; Fax +33 3 68 85 04 02; mail fdelay@unistra.fr

Abstract

Single and multiphase flows in fractured porous media at the scale of natural reservoirs are often handled by resorting to homogenized models that avoid the heavy computations associated with a complete discretization of both fractures and matrix blocks. For example, the two overlapping continua (fractures and matrix) of a dual porosity system are coupled by way of fluid flux exchanges that deeply condition flow at the large scale. This characteristic is a key to realistic flow simulations, especially for multiphase flow as capillary forces and contrasts of fluid mobility compete in the extraction of a fluid from a capacitive matrix then conveyed through the fractures. The exchange rate between fractures and matrix is conditioned by the so-called mean matrix block size which can be viewed as the size of a single matrix block neighboring a single fracture within a mesh of a dual porosity model.

We propose a new evaluation of this matrix block size based on the analysis of discrete fracture networks. The fundaments rely upon establishing at the scale of a fractured block the equivalence between the actual fracture network and a Warren and Root network only made of three regularly spaced fracture families parallel to the facets of the fractured block. The resulting matrix block sizes are then compared via geometrical considerations and

two-phase flow simulations to the few other available methods. It is shown that the new method is stable in the sense it provides accurate sizes irrespective of the type of fracture network investigated. The method also results in two-phase flow simulations from dual porosity models very close to that from references calculated in finely discretized networks. Finally, calculations of matrix block sizes by this new technique reveal very rapid, which opens the way to cumbersome applications such as preconditioning a dual porosity approach applied to regional fractured reservoirs.

Keywords

Fractured porous media; Matrix block sizes; Dual porosity models; Multiphase flow.

1. Introduction

Conventional oil reservoirs are often housed in fractured rocks, especially in carbonates environments, and one can estimate that more than 30 % of world oil reserves are concealed in densely fractured systems, oil being mainly trapped in the host rock matrix. Paradoxically, these geological structures may trigger contrasted effects on large-scale two-phase flow patterns by increasing oil recovery due to high local permeability values, or on the opposite, by decreasing oil extraction rates because of early water invasion, viscous fingering etc. The same type of behavior is also encountered in the context of water decontamination and can become even more complex if oil (and/or water) is swept by injections of miscible gas.

Modeling two-phase flow in fractured reservoirs is now often employed for the purpose of various applications, for instance to assess the relevance of different oil recovery strategies or to investigate on the feasibility of in-situ water decontamination processes (Bourbiaux, 2010). This fact makes that modeling single phase or multiphase flow in fractured media is still a fertile research domain even though pioneering works on the topic started in the early sixties (e.g., in Lemonnier et al., 2010a, b).

In this context, flow simulations relying upon finely gridded discrete fracture networks and their associated (discretized) matrix blocks are becoming increasingly popular because of the availability of high performance computers, the progress in algorithms for meshing complex geometries, and the availability of sophisticated numerical techniques for solving partial differential equations (Landereau et al., 2001; Noetinger et al., 2001; Adler et al., 2005; Matthäi and Nick, 2009; Fourno et al., 2013). This exhaustive approach is critical to bring us reference solutions and various benchmarks with which simpler approaches can be compared. Nevertheless, gridded discrete fracture networks may be poorly documented and include flawed information in the case of real-world applications. In addition, finely gridded

systems remain hardly usable for current practical applications to large-scale systems that result in cumbersome model parameterizations and heavy computations. This downside is emphasized in the domain of petroleum engineering usually dealing with both non-linear multiphase flow and dense fracture networks requiring huge discretization efforts (Landereau et al., 2001; Adler et al., 2005; Fourno et al., 2013). Applicability is also hindered by duplicated calculations if the study encompasses tests of various model designs, various model parameterization and various flow scenarios.

Fortunately, dense fracture networks are also good candidates to homogenization at the scale of reasonable elementary mesh sizes (on the order of 5-100 m) by resorting for example to the dual porosity approach to fractured media initially developed by Barenblatt et al. (1960). The dual porosity formulation conceptualizes a fractured system as two overlapping continua merging a fracture medium and a matrix medium with contrasts of hydraulic properties between the two continua. Flow is then described by a set of equations in each continuum (this set depends on the type of flow and the fluid phases present in the system) associated with an exchange term ruling the fluid fluxes percolating between continua.

This exchange term is all the more important that in general fractures are conveying flow as the matrix stores fluid volumes. In transient problems as for example forced flow between injecting and extracting wells, the way the relationship establishes between storage capacity and conduction property conditions the overall response of the reservoir (e.g., Acuna and Yortsos, 1995). In the specific cases of two-phase flow (water and oil), the absence or the weak incidence of capillary forces in open fractures makes that flow is locally mainly of single-phase type conveying either oil or water (with sharp saturation fronts in between) at different locations in the fracture network. For its part, the way the matrix blocks are soaked (water invades the matrix and pushes oil away) or drained (oil pushes water) strongly depends

on matrix block sizes and on the petro-physics properties of the matrix, making that extraction from the matrix of a fluid by the other is mainly driven by capillary forces or by capillary forces plus viscous forces (single-phase Darcian flow to make it simple).

When a discrete fracture network is connected enough and handled at an elementary scale larger than a representative elementary volume, the exchange term in the dual porosity models is proportional to an equivalent matrix block size. Intuitively, a REV for a fracture network is a volume within which mean properties of the network such as fracture density, fracture aperture, fracture hydraulic conductivity have some statistical meaning (Long et al., 1982; Neuman, 1988). In a dual porosity model, the REV is also associated with the capability to represent the actual fracture network as a synthetic network made (in three-dimensional problems) of three regularly spaced fracture families, each family developing fracture planes normal to one of the three main directions of flow. The so-called DFN homogenized as a "sugar-cube" model (Warren and Root, 1963) is at the origin of the notion of the equivalent matrix block size in relation with the dimensions of the elementary "sugar piece" separating neighbor fractures in the homogenized DFN (Kazemi et al., 1976).

There exist two types of methods to evaluate the elementary matrix block size. The first type relies upon exercises matching actual well test drawdown curves with analytical solutions that inherit from rigorous mathematical homogenization or large-scale averaging techniques (Arbogast 1990; Quintard and Whitaker, 1993; Noetinger et al., 2001; Unsal et al., 2010; Noetinger and Jarrige, 2012). The downside of these techniques is that sometimes actual well testing in fractured rock do not exist and when these tests exist, the damaged zone in the close vicinity of a well may not fully reflect flow conditions in the natural fracture network. The second type of methods is based on geometrical considerations regarding the fracture network. These considerations led to three geometrical approaches that are the geometrical imbibition method (GI, Bourbiaux et al., 1997), the enhanced general imbibition

method (EGI, Bourbiaux et al., 2006), and the mean spacing method (MS, Narr, 1996). It is obvious that these approaches can only be applied if a minimum prior knowledge about the fracture network geometry is available.

In this contribution we propose a new geometrical method that can to some extent overlook the actual geometry of the fracture network because the method relies upon the identification of a sugar-cube DFN equivalent to the actual network (see details hereafter). The method also allows us to calculate matrix block sizes along directions parallel to the main flow directions that are conditioned by the geometry of the fracture network (or its equivalent as a sugar-cube model). Section 2 (and Appendix A) is focused on the theoretical framework we rely upon to build the so-called oriented block size (OBS) method that we propose. For the sake of clarity, a few features about dual-porosity models are also reminded. The matrix block sizes stemming from the OBS technique are then compared to that from the other geometrical techniques (GI, EGI, and MS, see above). The comparison is performed by way of a suite of calculations applied to synthetic random fracture networks for which we explicitly control both the geometric and hydraulic properties of the networks and the mean size of matrix blocks between fractures. As told earlier, only dense and well-connected fracture networks are considered because sparse networks cannot be homogenized via a dual porosity model at the scale of a complete underground reservoir. Section 4 evaluates the OBS technique and also the other geometrical approaches within the framework of a dual-porosity model compared with exhaustive calculations discretizing the fracture network and the matrix blocks. The two-phase flow scenarios are either dominated by capillary forces or viscous forces in an exercise which consists in draining oil from matrix blocks by injecting water in fractures. These complex flow scenarios are performed over synthetic test cases in which we control the reference calculations (in a fully discretized system). This procedure enable us to clearly

emphasizes the main theoretical findings regarding matrix block size in dual porosity models before envisioning further concrete field-scale applications.

2. Theoretical background

In various approaches to fractured systems, the duality of fracture networks embedded in a host rock matrix is often represented as two overlapping continua merging a fracture medium and a matrix medium. In a so-called dual porosity – single permeability model, the fractures are usually highly conductive and poorly capacitive as the matrix is highly capacitive but with negligible flow triggered by fluid pressure gradients (weak permeability). As an example, single-phase Darcian flow in a dual continuum approach results in the resolution of two equations in the form

$$\frac{\partial\left(\rho\phi^{f}\right)}{\partial t}+\nabla.\left(-\rho\frac{\mathbf{k}^{f}}{\mu}.\nabla\left(P^{f}+\rho gz\right)\right)-E^{m\to f}=0 \qquad (1)$$

$$\frac{\partial\left(\rho\phi^{m}\right)}{\partial t}+E_{p}^{m\to f}=0 \;\; ; E_{p}^{m\to f}=\rho\sigma\frac{\mathbf{k}^{m}}{\mu}\left(P^{m}-P^{f}\right) \qquad (2)$$

For the sake of simplicity, references to space (x) and time (t) for parameters and state variables have been dropped. The indexes f and m refer to fracture and matrix continua, respectively. ρ [ML-3] is the mass density of the fluid, μ [ML-1T-1] is the dynamic viscosity of the fluid, $\mathbf{k}^{\lambda}$ [L2] is the permeability of the continuum λ $(\lambda=f,m)$, ϕ^{λ} [-] is the porosity of the continuum λ, P^{λ} [ML-1T-2] is the fluid pressure in the continuum λ, g [LT-2] is the scalar value of the gravity acceleration g, and z [L] is the local elevation taken from an arbitrary reference and counted positive upward. $E_{p}^{m\to f}$ [$ML^{-3}T^{-1}$] is the exchange rate (a mass fluid flux per unit volume of medium) between the fracture and the matrix continua.

In (2), the exchange rate is of pseudo steady-state type meaning that the relationship between matrix and fractures depends on pressure gaps between the continua and not on a convolution product of their derivatives with respect to time. In (2), the matrix permeability $\mathbf{k}^m$ is assumed small enough to neglect Darcian fluxes in the matrix (compared to that in the fractures) but large enough to enable fluid flux percolation between the matrix and the fractures. Therefore, the matrix permeability is an entry of the exchange rate via the term $\sigma\mathbf{k}^m, \sigma$ [L^{-2}] being a shape factor tensor that quantifies the mean size of the matrix blocks associated with the fractures included in an elementary volume (for example, the volume corresponding to the elementary meshing employed when solving numerically Eqs (1) and (2)). By construction, the pseudo steady-state assumption in (2) ignores the early transient flow regime between matrix and fractures which may result in erroneous evaluations of exchanged fluid fluxes, especially in the case of weakly permeable matrix media requiring long times for equilibrating their fluid pressure fields with that of fractures (e.g., as in shale gas and shale oil extraction problems). Transient exchange rates between fractures and matrix are the natural outcome of Multiple INteracting Continua (MINC approaches) initially developed in the late eighties (e.g., Pruess and Narasimhan, 1985; Pruess et al., 1990) and more recently reassessed and improved (e.g., Karimi-Fard et al., 2006; Tatomir et al., 2011, de Dreuzy et al., 2013). The MINC models are not incompatible with the notion of mean matrix block size in homogenized fractured systems as each matrix block is viewed as an entity of prescribed size enclosing a nested heterogeneity.

Various formulations of the shape factor have been proposed for many modeling applications (Kazemi et al., 1976; Thomas et al., 1983; Coats 1989; Ueda et al., 1989; Lim et al. 1995; Quintard and Whitaker, 1996; Noetinger and Estebenet., 2000) amongst which the formulation proposed by Kazemi et al. (1976) is the one used in this study. This choice is motivated by a quite simple formulation which allows for dealing with diagonal tensors, and

also introduces the mean matrix block size as a quantity weighting the influence of the matrix permeability tensor to control the fluid fluxes exchanges between matrix and fractures. For diagonal permeability and shape factor tensors, the product $\boldsymbol{\sigma}\mathbf{k}^m$ is developed as

$$\boldsymbol{\sigma}\mathbf{k}^m = \begin{pmatrix} k_x^m / s_x^2 & 0 & 0 \\ 0 & k_y^m / s_y^2 & 0 \\ 0 & 0 & k_z^m / s_z^2 \end{pmatrix} \quad (3)$$

with s_i [L] (i=x, y, z) the mean matrix block size along the main flow direction i. As the exchange rate between the fractures and the matrix is a key feature to the behavior of a dual continuum and some other homogenized approaches (Lemonnier et al., 2010a, b), it makes sense to revisit the item especially regarding the mean matrix block size (which rules the fluxes, provided the fluid pressure fields are correctly calculated).

The Oriented Block Size (OBS) technique that we develop below infers the mean matrix blocks sizes s_i (i=x, y, z) from a fractured system by assuming that a rock block enclosing an actual fracture network with various characteristics (e.g., Fig 1) can be turned into a simplified block with an equivalent fracture network composed of three families of planar fractures.

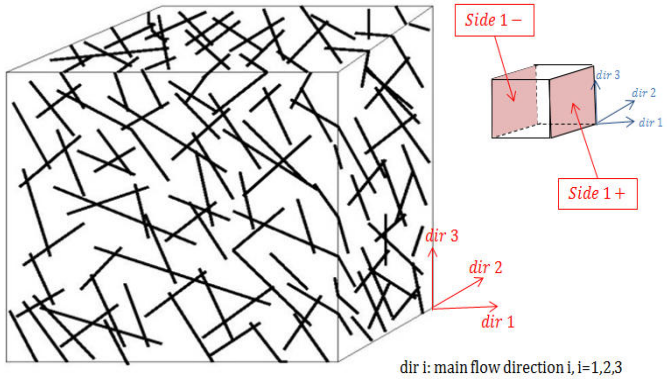

Fig. 1. A fractured rock block at the scale of a reservoir grid cell with references to main flow directions and facets of block normal to flow directions.

Each family is defined by a uniform spacing between fractures and a fracture plane normal to one direction of flow (or including the two other directions). This equivalent fracture network (e.g., Fig. 2) which draws the so-called "sugar-cube" configuration as proposed by Warren and Root (1963) and referred to as the WR model hereafter, is conceptually compatible with the notion of mean matrix block size. The three families of WR fractures delimit a parallelepiped elementary block separating neighbor fractures that should coincide with the shape factor as defined in Eq (3). If the whole WR block is wide enough, the three fracture families can be aggregated as a single fracture permeability tensor (or value) and a single fracture porosity for the whole block or its facets. These parameters depend on the size of the elementary matrix block separating the WR fractures. By comparing, or more exactly by identifying permeability and porosity properties of a WR block with that of an actual fractured block, one is able to define the equivalent mean matrix block size of the actual fractured block.

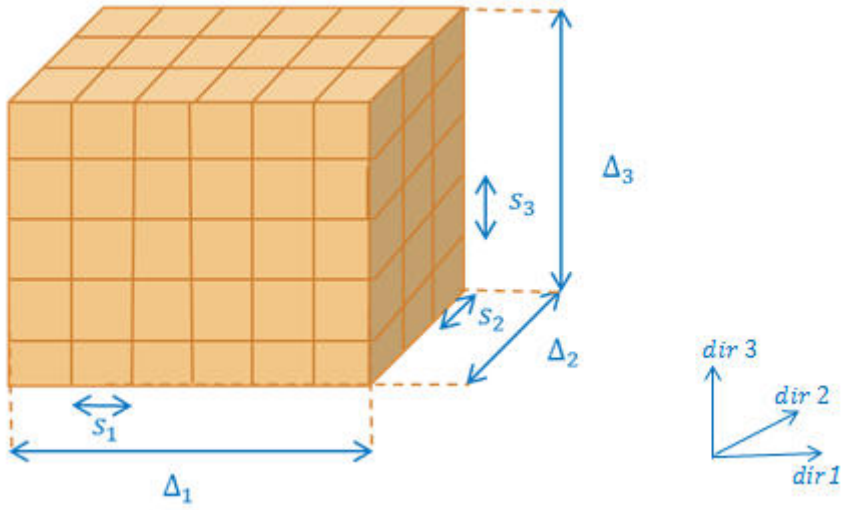

Fig. 2. A regular fracture network of three fracture families (a Warren and Root (WR) model) at the scale of a reservoir grid cell with reference to main flow directions, facets of block normal to flow directions, and spacing between fractures.

Let us take a parallelepiped block housing an actual fracture network as depicted in Fig. 1. The first way to identify a single macroscopic permeability tensor $\mathbf{k}^f$ for the block is to employ upscaling approaches, multiple continua theory (Karimi-Fard et al., 2006; Tatomir et al., 2011; Jourdain et al., 2014), analytical solutions (Oda, 1985) or simply to conjecture the entries of the tensor as could be done, for example, in parameterizing a dual porosity approach after having postulated that the approach was convenient for the problem under investigation. A second way is to extract the (diagonal) tensor from the structural properties of the fracture network and its relationships with the homogenization volume (the block) concealing it.

The actual fractured block as depicted in Fig 1 is oriented with its main directions along the main directions of flow indexed by *i*=1,2,3 (here completely equivalent to $i = x, y, z$ for locations in space denoted $\mathbf{x} = (x, y, z)$ but easier to manipulate when incrementing the index). The block size in direction i is denoted Δ_i and the sides delimiting the block are also indexed by i but for limits normal to the main direction i. In addition, block sides are labelled $i-$ or $i+$ according to their respective location upstream or downstream along direction i. Assuming that the fractured block is well connected, the mean permeability of the block along a direction i can be calculated as the average over the sides $i-$ and $i+$ of the local permeability of fractures intercepting the sides. This yields

$$k_i^{FN-S} = \frac{1}{2\left(\Delta_{i+1}\Delta_{i+2}\right)}\left(\sum_{n=1}^{Nf_{i-}} k_n l_n e_n + \sum_{n=1}^{Nf_{i+}} k_n l_n e_n\right) \quad (4)$$

In the above equation, *i* is a cycling index such that, e.g., *i*+1 = 3 when *i* = 2 and *i*+1 returns to 1 when *i*=3. k_i^{FN-S} [L^2] is the macroscopic fracture permeability of the fractured block along direction *i*, $\Delta_{i+1}\Delta_{i+2}$ [L^2] is the total surface area of sides $i-$ and $i+$ these being intercepted by a number of fractures Nf_{i-} and Nf_{i+}. k [L^2] is the local permeability of a

fracture seen as intercepting the side of the block over an apparent length *l* and with apparent fracture aperture *e* [L].

By re-using the same notations for directions and sides in a rock block modeled as a WR network (Fig. 2), one can also calculate the entries k_i^{WR} of the diagonal fracture permeability tensor of the WR block along directions i. The three fracture families of the WR network are also indexed by i with the same notation as for the block sides, i.e., a fracture family i corresponds to fracture planes normal to direction i. A family i is of uniform spacing s_i [L] (s_i is measured along direction i, see Fig. 2), counts Nf_i fractures with a uniform scalar permeability k_i and a uniform fracture aperture e_i. With these settings and the assumption that flow only occurs in the fractures, the total flow rate entering or exiting the WR fractured block through a side *i* normal to the direction *i* can be expressed as

$$Q_i = -\nabla_i P\left(\sum_{j\neq i} Nf_j e_j \Delta_{k;k\neq i,k\neq j}\frac{k_j}{\mu}\right) = -\nabla_i P\frac{k_i^{WR}}{\mu}\Delta_{i+1}\Delta_{i+2} \qquad (5)$$

For the sake of simplicity, the gravity components of flow have not been accounted for in (5). $Nf_j e_j \Delta_{k;k\neq i,k\neq j}$ represents the total surface of flow developed by the family fracture *j* through the side *i* of the block, $\Delta_{i+1}\Delta_{i+2}$ is the total surface area of the side *i*, and k_i^{WR} is the macroscopic fracture permeability of the WR block along direction *i*. The equality in (5) comes down to a direct identification of the three terms of the macroscopic permeability $\mathbf{k}^{WR}$ as

$$\begin{bmatrix} k_1^{WR} \\ k_2^{WR} \\ k_3^{WR} \end{bmatrix} = \begin{bmatrix} 0 & 1/\Delta_2 & 1/\Delta_3 \\ 1/\Delta_1 & 0 & 1/\Delta_3 \\ 1/\Delta_1 & 1/\Delta_2 & 0 \end{bmatrix} . \begin{bmatrix} Nf_1 e_1 k_1 \\ Nf_2 e_2 k_2 \\ Nf_3 e_3 k_3 \end{bmatrix} \qquad (6)$$

In the context of scaling the values k_i^{WR} so they become equivalent to calculated values in a rock block encapsulating an actual fracture network, the number Nf_i of WR fractures, their

aperture e_i and their permeability k_i become the unknowns of the problem. Therefore, it makes sense to invert the linear system of equation (6) which yields

$$Nf_i e_i k_i = \frac{\Delta_i}{2} \sum_{j=1}^{3} (-1)^{\delta_{i,j}} k_j^{WR} \tag{7}$$

with $\delta_{i,j}$ the Kronecker delta function, $\delta_{i,j} = 1$ if $i = j$ and $\delta_{i,j} = 0$ if $i \neq j$.

By considering the structure of a WR fracture network, one can write

$$Nf_i \left(e_i + s_i \right) = \Delta_i \;\Rightarrow\; \frac{Nf_i e_i}{\Delta_i} = \frac{e_i}{e_i + s_i} \tag{8}$$

Note in the above expression that counting Nf_i fractures assumes the presence of $Nf_i - 1$ fractures inside the block and that the two sides *i* of the block are each bounded by half a fracture of family *i* with half the aperture e_i counted in the block. Introducing (8) in (7) results in

$$k_i = \frac{1}{2}\left(1 + \frac{s_i}{e_i} \right) \sum_{j=1}^{3} (-1)^{\delta_{i,j}} k_j^{WR} \tag{9}$$

The expression (9) will be used later for the purpose of identification between an actual fractured block and a WR block.

Let us look at the porosity properties of the WR block. The fracture porosity ϕ^{WR} [-] of the whole WR block and the fracture density ϕ_i^{WR-S} [-] at a side *i* defined as the porosity of fracture network at a side of the block (the ratio of the surface area of open fractures at a side to the total surface of the side) can also be derived as

$$\phi^{WR} \approx \sum_{i=1}^{3} \frac{Nf_i e_i \Delta_{i+1} \Delta_{i+2}}{\Delta_1 \Delta_2 \Delta_3} = \sum_{i=1}^{3} \frac{Nf_i e_i}{\Delta_i} \tag{10}$$

$$\phi_i^{WR-S} \approx \sum_{l \neq i} \frac{Nf_l e_l}{\Delta_l} \tag{11}$$

Notably, the expressions in (10) and (11) are rather simple but are approximations since the intersections of fractures are counted twice in the porosity values. This was found of negligible influence for classical block sizes and fracture apertures. Subtracting (11) from (10) returns the term $Nf_i e_i/\Delta_i$ which also appears in Eq (8). Therefore, another way to express the relationship between the local WR fracture permeability k_i and the macroscopic permeability $\mathbf{k}^{WR}$ in (9) is

$$k_i = \frac{1}{2\left(\phi^{WR} - \phi_i^{WR-S}\right)} \sum_{j=1}^{3} (-1)^{\delta_{i,j}} k_j^{WR} \tag{12}$$

Both expressions (9) and (12) are employed to define the matrix block size s_i (in 9).

If the WR network is equivalent regarding its hydraulic properties to the actual fracture network, it is expected that ϕ^{WR}, ϕ_i^{WR-S}, and k_j^{WR} are similar to the equivalent properties in the actual block of fracture network, respectively denoted as ϕ^{FN}, ϕ_i^{FN-S}, and k_j^{FN-S} (see (4) for the latter term). It is also expected that the WR network, while being still equivalent to the actual fractured block, can inherit some properties (parameters) of a homogenized model such as the mean matrix block sizes of the medium and the permeability tensor at the macroscopic scale of a fractured block. By imposing these properties in (9) and (12), and after a few algebraic manipulations (see Appendix A for details), an expression of the mean matrix block sizes in a homogenized fractured block can be written as

$$s_i \approx \frac{\sum_{j=1}^{3} (-1)^{\delta_{i,j}} k_j^{FN-S}}{\left(\phi^{FN*} - \phi_i^{FN-S*}\right) \sum_{j=1}^{3} (-1)^{\delta_{i,j}} k_j^{f}} \tag{13}$$

$k_i^{FN-S}\ (i = 1,2,3)$ are the permeability values at the sides i of the actual fractured block, $k_i^{f}\ (i = 1,2,3)$ are the entries of the diagonal permeability tensor of an homogenized medium equivalent to the fractured block (e.g., that of a dual porosity model), and ϕ^{FN*} ,

$\phi_i^{FN-S*}\ (i=1,2,3)$ are rescaled block and side porosities of the actual fractured block. These rescaled porosities of dimension [L^{-1}] (a porosity per unit fracture aperture) are calculated over the skeleton of the actual fracture network to which each fracture is assigned a unit fracture aperture.

In addition to postulating the equivalence between a WR block and the actual fractured block, the assumptions allowing us to derive (13) are twofold. First, the actual fracture network is a good candidate for homogenization with the meaning that there exist macroscopic properties as mean matrix block size and diagonal permeability tensor characterizing the hydraulic behavior of the network at the large scale (at least, the scale of a mesh of a homogenized model). Second, a WR network exists (as that investigated by way of equations 5 to 12) but with uniform fracture aperture e_f over its three fracture families and still equivalent to the actual fracture network (see Appendix A for details). There is no clear criterion (except dealing with a dense and well-connected network) allowing us to state beforehand whether or not a given fracture network would follow the above assumptions. Eventual criteria would also depend on the flow processes and mechanisms targeted for further applications at the large scale.

It is worth to note that Eq. (13) depends on both the facet permeability values of the actual fractured block k_j^{FN-S}, and the structural properties of the actual fracture network skeleton in the form of porosities ϕ^{FN*} and ϕ_i^{FN-S*}. These features make that applicability of (13) is conditioned by a good knowledge of the actual fracture network geometry and, as a downside, renders the method hardly applicable to poorly-known natural systems. In the end, Eq. (13) should be mainly used in problems dealing with homogenization of systems with well-known geometry and discretization of synthetic fracture networks (as done for instance in reservoir engineering when passing from a geological model to a tractable flow model).

326 This notwithstanding, the OBS technique can also deliver another form of the mean
327 matrix block size. By manipulating the expression of the side block permeability of the actual
328 fractured block in (4), scaling the subsequent expression with the side block porosities ϕ_i^{FN-S}
329 and making use of (13) (details are provided in Appendix A), another form of the mean matrix
330 block size comes up as

331 $$s_i \approx \frac{2e_f \overline{k}}{\sum_{j=1}^{3}(-1)^{\delta_{i,j}} k_j^f} \qquad (14)$$

332 This form introduces the existence of a mean single fracture aperture e_f [L] (which is also the
333 uniform aperture mentioned above for the WR network) and a mean single-fracture
334 permeability $\overline{k}$ [L^2] at the scale of the whole actual fractured block. These two quantities are
335 additional assumptions to that discussed regarding (13) for the applicability of (14).

336 Even though these assumptions may appear very restrictive, they give the possibility
337 to infer mean matrix block sizes from poorly known and hardly accessible fracture networks
338 as often encountered in field case applications. The entries k_j^f of the permeability tensor of
339 the whole fractured block can be evaluated by way of hydraulic tests; preferably interference
340 testing between distant wells that avoid bias stemming from an environment close to the
341 tested well that would not be representative of the fracture network at a larger scale. Values of
342 uniform single-fracture aperture e_f and uniform single-fracture permeability $\overline{k}$ are harder to
343 infer because data obtained for instance from optic imaging of boreholes (for e_f) and flow or
344 production logs (for $\overline{k}$) may reveal not representative of the whole network. It remains that
345 the matrix block size calculation in (14) is feasible without resorting to any knowledge on the
346 structure of the actual fracture network. It is obvious that the subsequent inferred value of
347 mean matrix block size should be taken as an order of magnitude (then refined for instance by
348 model inversion) instead of a robust pinpoint value.

In the following comparing: 1- the OBS technique with other geometrical techniques, and 2- the dual porosity approach (handling matrix block sizes s_i) with finely discretized networks, we address the relevance of the simplified expression in (14) under the assumption that the skeleton of the fracture network is known (as is the case with other geometrical methods). We prescribe to each fracture a uniform aperture and a uniform fracture permeability. The skeleton is then discretized and the entries k_j^f of the permeability tensor are calculated by performing numerical "permeameter" experiences (i.e., calculating fluid fluxes between opposite facets of the fractured block under prescribed Dirichlet boundary conditions while the other facets of the block are of no-flow type).

3. Comparison with structural-geometrical approaches

As shown from a theoretical standpoint, the OBS technique defines a mean matrix block size as a measure drawn from geometrical and structural properties of a discrete fracture network and its equivalent representation via a regular "sugar cube" network. In theory, no reference to any calculation of flow at the large scale is evoked in obtaining the OBS matrix block size, which renders the technique comparable in its spirit to other previous approaches also based on geometrical-structural characteristics of the discrete fracture network.

In the following, the OBS evaluation of matrix block sizes is compared with three other types of geometrical calculations, namely: the geometrical imbibition (GI) technique (Bourbiaux, 1997), the extended geometrical imbibition (EGI) technique (Bourbiaux et al., 2006), and the mean spacing (MS) technique (Narr, 1993). The main backgrounds of GI, EGI, and MS are summarized (sometimes slightly enhanced, as for EGI) and presented with notations consistent with that of the present work in Appendix B. GI and EGI techniques are only applicable (in their original version) to two-dimensional fracture networks and model the distance between any location in the matrix and the nearest fracture of the DFN. MS is

available for two- and three-dimensional systems and infers the mean lag distance between two neighbor fractures along the main directions of flow in a fractured block. All the geometrical methods need the detailed geometry of the DFN, although OBS could be used without it (See Section 2). But for a fair comparison we assume for all methods that the skeleton of the fracture network is known.

The comparison of OBS, GI, EGI, and MS is conducted for the two horizontal directions of a three-dimensional fractured block (100 m on a side) consisting of two families of near-vertical fracture planes. In the first test, a fracture family denoted *A*, is oriented with an azimuth of 100° counted positive anticlockwise from the main direction *x* of the fractured block. The second fracture family denoted *B* is oriented 10°.The spacing between fractures of family *B* is kept constant at 7 m, as the spacing of family *A* is varied between 2 and 8 m for different realizations of the DFN (two examples reported in Fig. 3).

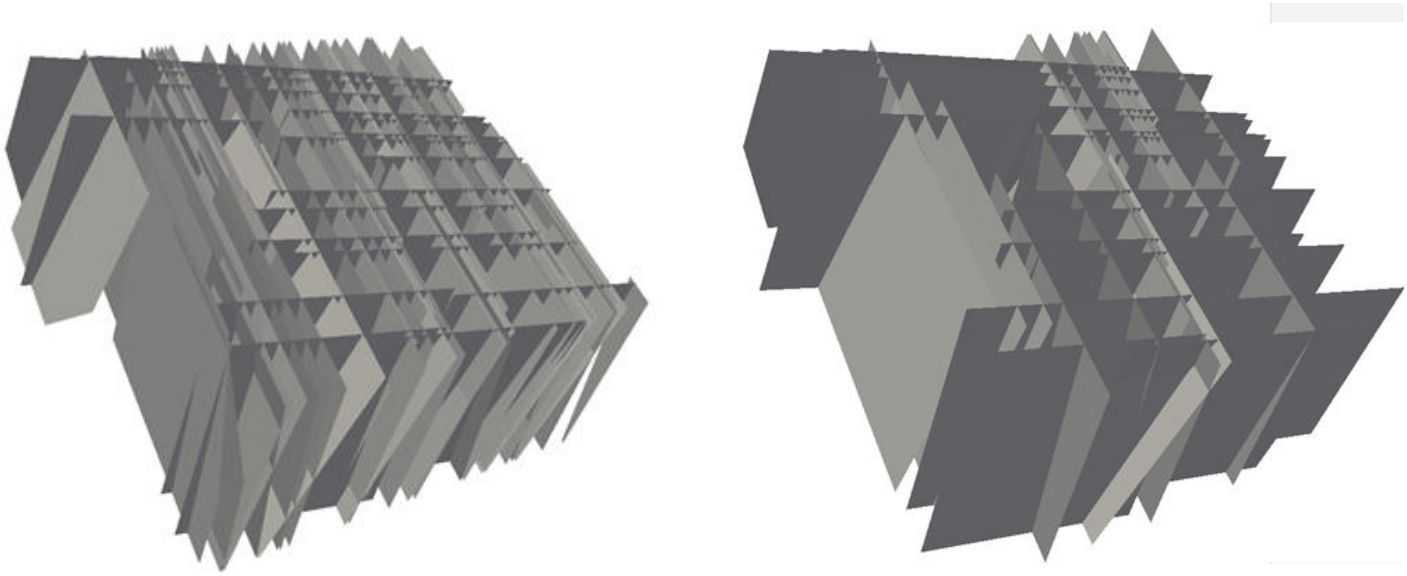

a **b**

Fig. 3. Examples of random discrete fracture networks (DFN) with two near-vertical fracture families at the scale of a reservoir grid cell. The azimuths of family *A* and *B* are 100° and 10°, respectively. DFN a: family *A* (resp. *B*) with mean spacing of 2 m (resp. 7 m); DFN b: families *A* and *B* with mean spacing of 7 m.

If we denote as s_x and s_y the mean matrix block sizes along the *x* and *y* horizontal directions of the fractured block, in view of the orientations of fracture families *A* and *B*, s_x should be close to the mean spacing of *A* (i.e., 2 – 8 m), and s_y close to the spacing of *B* (i.e., 7 m). Fig. 4 reports on sought values of s_x and s_y for different methods of calculation with specifically the EGI technique rendering two sets of measures (see Appendix B) - small-EGI, large-EGI – as the technique assumes the existence of two types of matrix block interacting with the fracture network during flow.

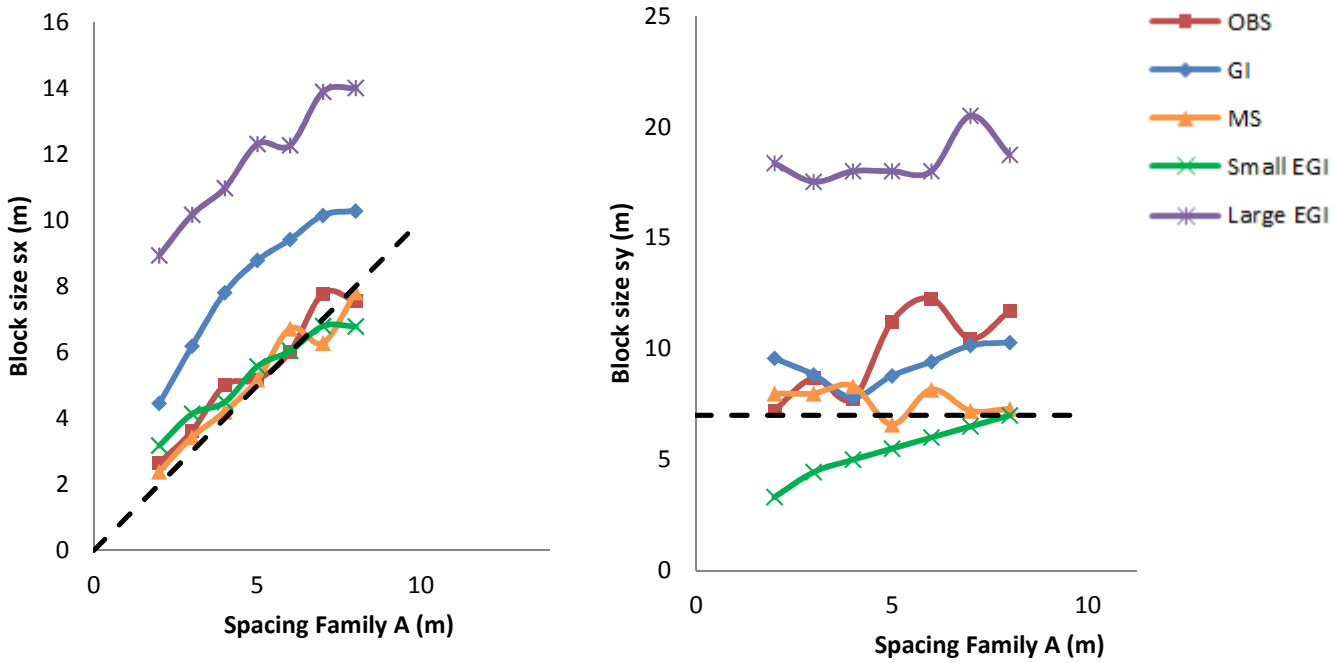

a **b**

Fig. 4. Mean matrix block sizes s_x and s_y as functions of the spacing of fracture family *A* (fracture networks in Fig. 4) for different methods of calculation. OBS = oriented block size method, GI = general imbibition method, EGI = enhanced general imbibition method (with "small" and "large" sizes of matrix blocks), and MS = mean spacing method.

In general, the OBS calculations retrieve the expected values of $s_x \approx 2-7\,\mathrm{m}$ as a function of the spacing of fracture family *A* (Fig. 4a). The size s_y which should be constant at

405 7 m, actually evolves with the spacing of family *A* and is overestimated of 10% to 50% (Fig.
406 4b). This overestimation cannot be the consequence of an actual fracture network that would
407 be far from a regular WR representation since the actual network is simple and made of two
408 perpendicular fracture families with directions almost parallel to the *x* and *y* directions of the
409 fractured block. Nevertheless, we noted that increasing the spacing of the fracture family *A*
410 also diminished the connectivity of the DFN with a few subdomains almost free of any
411 fracture and poorly connected to the facets of the fractured block. It is noteworthy that
412 estimates of effective properties of the DFN, especially porosities (or their influence on
413 macroscopic permeabilities in Eq. (15)), both at the facets and inside the block are key
414 features to the OBS calculations (see Section 2). Since less connected networks return weaker
415 porosity values, the equivalent WR network assigned with those porosities will contain less
416 fractures and result in increased matrix block sizes extracted from the equivalence between
417 the WR network and the DFN.

418 Compared with the expected values, matrix block sizes s_x and s_y extracted from the
419 GI technique tend to be overestimated. This result is foreseeable because GI usually
420 experiences some difficulties when dealing with DFN encompassing both small and large
421 matrix blocks. These difficulties are the consequence of the oversimplified fitting with a
422 second degree polynomial of the so-called invasion area curve calculated by the method as the
423 surface area in the matrix domain located at a given distance from the closest fracture of the
424 system (see Appendix *B*). Regarding EGI, the "small block" estimates s_x are in the correct
425 range 2-8 m when the size s_y is always overestimated. For their part, the "large block"
426 estimates in EGI are always more than twice the expected values. Finally, the MS method
427 infers correct values of s_y and s_y whichever the investigated DFN and the spacing of fracture
428 families *A* and *B*. Notably, the MS method is weakly influenced by the fracture network
429 connectivity which might become a drawback when dealing with sparse and poorly connected

fracture networks. In that case MS will still measure the mean lag distance separating two neighbor fractures, as a poorly connected network tends to conceal a few cluster of large matrix blocks in the system. In that case mean matrix block sizes from MS would be underestimated.

In the OBS technique, whose specificity is seeking the equivalence between the actual DFN and a regular WR network, this equivalence seems intuitively easier to achieve for DFNs with fracture families whose principal orientations are close to the main directions of the whole block. Therefore, it makes sense to address the capabilities of the method under less favorable conditions where actual fractures do not line up with the main block directions. We re-handled the comparison of matrix block sizes drawn from fracture networks still made of two almost vertical fracture families, but this time with a constant spacing of 3 m for family *A*, 5 m for family *B*, and varying the orientation of the families with respect to the main directions *x* and *y* of the block. The fracture family *A* is still oriented 100° (counted positive anticlockwise) with respect to the *x* direction and the orientation of family *B* is varied between 0 and 70° with respect to *x* (Fig. 5). In view of the geometrical settings of the DFNs, the matrix block size s_x should be close to 3 m and s_y close to 5 m when the fracture family *B* is almost orthogonal to family *A* (azimuth of *B* = 0-10°). Block sizes s_x should then slightly decrease as s_y should increase when the direction of fracture family *B* departs from orthogonality with *A*.

The GI method systematically overestimates both s_x and s_y in each configuration of the fracture network. The EGI technique still tends to overestimate s_x and s_y with its "large block" measure while correct or slightly underestimated values are found with the "small block" measure. In any case, both GI and EGI are weakly sensitive to the fracture family orientations with almost constant values s_x and s_y irrespective of the azimuth prescribed to

fracture family *B* in the DFN (Fig. 6). This result is consistent with the fact that both techniques model the surface occupied by matrix domains in the fractured block as a function of the distance to the nearest fracture (Appendix B). This measure reveals far less sensitive to fracture orientations than to fracture spacing.

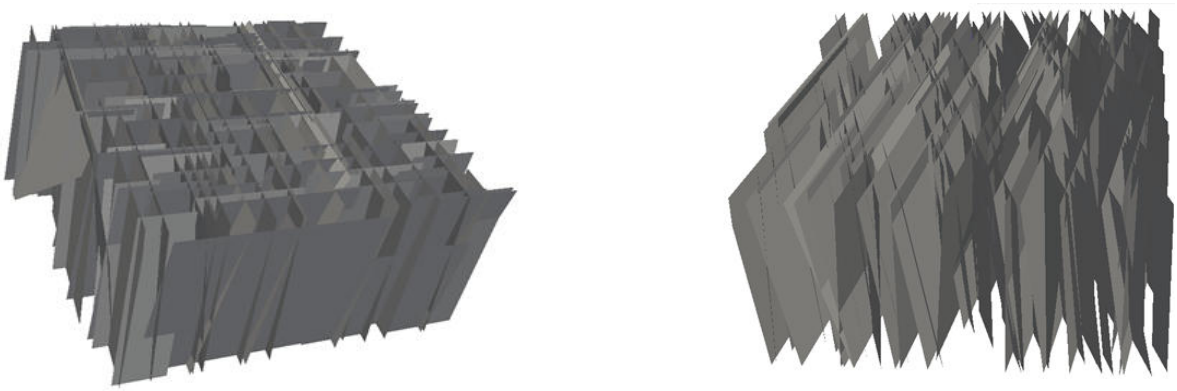

a **b**

Fig. 5. Examples of random discrete fracture networks (DFN) with two near-vertical fracture families at the scale of a reservoir grid cell. The mean spacing of fracture families *A* and *B* are prescribed at 3 m and 5 m, respectively, while the azimuth of family *A* is kept at 100° and the azimuth of family *B* is varied between 0° (DFN a) and 70 ° (DFN b).

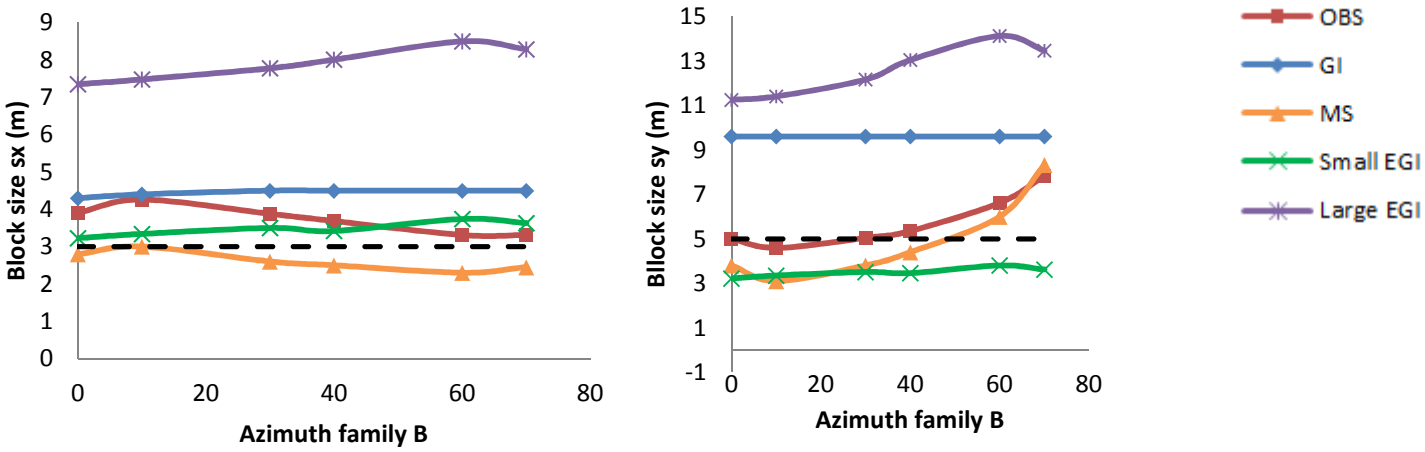

a **b**

Fig. 6. Mean matrix block sizes s_x and s_y as functions of the azimuth of fracture family *B* (fracture networks in Fig. 5) for different methods of calculation. OBS = oriented block size method, GI = general imbibition method, EGI = enhanced general imbibition method (with "small" and "large" sizes of matrix blocks), and MS = mean spacing method.

The MS and OBS techniques infer very similar matrix block size values, these being sometimes slightly underestimated by MS and slightly overestimated by OBS. For azimuths of the fracture family *B* between 0 and 45°, the estimated s_x with both MS and OBS are close to the expected value of 3 m and stay almost constant whichever the orientation of family *B*. Concerning s_y, the expected value of 5 m is retrieved by OBS and underestimated at 3-4 m by MS. For azimuths of the fracture family *B* between 45 and 70°, both methods return, as expected, s_x values that slightly decrease, as s_y values increase from approximately 5 m up to 8 m. OBS mainly captures the projection of the fracture planes onto the facets delimiting the fractured block (see Section 2 and Appendix A), which is obviously sensitive to fracture orientations. In the same vein, MS evaluates the mean distance between fractures along the main directions of the fractured block with the obvious consequence of increasing the apparent distance when fracture planes are not normal to the direction of measure. Nevertheless, both methods provide valuable results for dense fracture networks or fractured blocks wide enough to enclose a large number of fractures allowing for significant statistical measures of fracture spacing (MS) or block-side and inner-block hydraulic properties (OBS).

Notwithstanding other considerations such as computation times (see hereafter), OBS and MS techniques seem to outperform GI and EGI in extracting mean matrix block sizes from fractured system. We noted however that OBS is sensitive to the loss of connectivity in a fracture network with the consequence of increasing the inferred matrix block size. This artificial increase might result in biased evaluations of fluid flux exchanges between fracture and matrix media. Numerical exercises comparing discrete fracture network outputs and their dual porosity representation with OBS-sized matrix blocks are conducted to answer this question. The other geometrical techniques GI, EGI, and MS are also tested. We remind that these three numerical techniques are in essence only applicable when a prior knowledge of the fracture network geometry is available, while the OBS technique might by applied either on

492 known or unknown geometries (see Section 2). For a fair comparison of all techniques
493 hereafter, we consider that the fracture network geometry is known.
494
495 **4. Two-dimensional numerical test cases**
496 As already mentioned, dual continua representations of discrete fracture networks are
497 conducive to drastic reductions in computation costs but require carefully designed settings to
498 adequately represent both conductive and capacitive properties of a fractured porous medium
499 subject to Darcian flow. We address here two phase flow in both DFN and dual porosity
500 models. The setup of calculations is dimensioned to represent large laboratory analogs of
501 flow in fractured media as conducted for instance in "Hele-Shaw" cells (e.g., Park and
502 Homsy, 1984; Folch et al., 1999). We remind that we are interested in the assessment of mean
503 matrix block size from different geometrical-structural techniques that always manipulate
504 relative quantities as the spacing of fractures compared to the block size, or fracture traces
505 intercepted by block facets. Therefore, our findings from numerical experiments at the scale
506 of a lab device should not be hampered by loss of generality. In addition, we perform
507 calculations, especially in the context of DFN discretization, over synthetic fracture networks
508 with regular fracture orientations. This choice reduces discretization efforts but is mainly
509 employed herein because it ensures accuracy of reference calculations in a DFN compared
510 with that from a dual porosity model. Even though sophisticated meshing techniques and
511 advanced numerical methods exist, it was found that thin fracture elements in unstructured
512 meshing tend to smear the calculation of their state variables over the large matrix blocks.
513 This feature is not suited to compare (local) DFN and (large scale) dual porosity calculations
514 of diffusive flow.
515 Numerical simulations are performed over two-dimensional horizontal fractured
516 systems (of unit thickness) that only neglect gravity-driven flow. Notably, the various

techniques employed in this study to calculate mean matrix block sizes are not sensitive to gravity-driven flow and only manipulate geometrical considerations on the fracture network or equivalences in permeability-porosity between an actual fractured block and a sugar-cube model. Two-phase flow in a DFN is performed over a fractured system of 3 m length and 1.5 m width finely discretized by 11590 square elements for an accurate representation of both the fracture network and matrix. The system is also roughly discretized by only 920 square elements of a dual-porosity, single-permeability model with matrix block sizes extracted from the DFN via the EI, EGI, MS and OBS techniques (see Section 3). Two-phase flow is numerically solved by means of a finite volume technique and uses an implicit-in-time scheme for time integration of the pressure equation while an explicit-in-time scheme is used for time integration of either the water or oil mass balance. To avoid unfair comparisons between GI, EGI, MS, and OBS, a simple fracture network is delineated with fractures only parallel to the main flow directions *x* and *y* of the system. Dead ends of the fracture network are also removed since in essence they are always accounted for in the fracture-matrix relationship by GI and EGI methods when MS and OBS might not see these dead-ends because they are not counted in MS or do not participate to side-block properties in OBS.

The first fractured system investigated (Fig. 7) is initially saturated with oil and percolated by water injected from the western boundary taken as a Neumann condition prescribing a constant-in-time water flux. The eastern boundary of the system is of Dirichlet type while North and South boundaries are of no-flow type. Table 1 indicates the local hydraulic properties of each medium (fractures, matrix) in the DFN, Table 2 reports on inner-block and block-side properties used by the OBS method to calculate matrix block sizes, and Table 3 gathers the various matrix block sizes s_x and s_y obtained from the GI, EGI, MS and OBS methods.

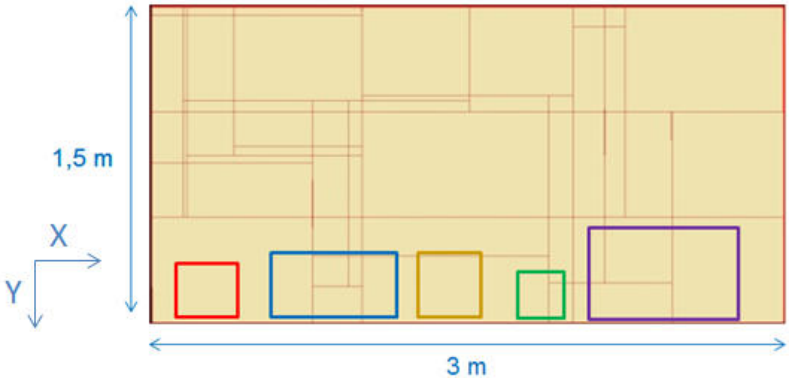

Fig. 7. Two-dimensional fracture network serving as a system finely discretized or handled as a dual-porosity model for the purpose of flow dynamics comparison. The size of matrix blocks in a dual porosity approach are reported as colored frames, from left to right: Red = oriented block size method, Blue = general imbibition method, Orange = mean spacing imbibition method, Green and Purple = small and large sizes from enhanced general imbibition method.

	Matrix medium	Fractures
Porosity ϕ [-]	0.1	1
Permeability k [10^{-15} m^2]	1 and 10	10000
Relative permeability k_r [-]	Brooks Corey (λ=2) 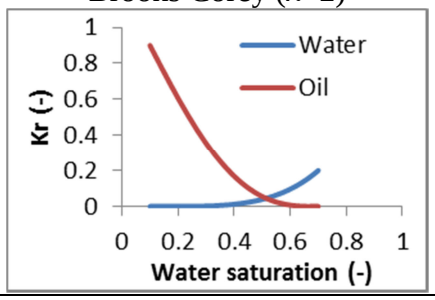	"Cross" k_r 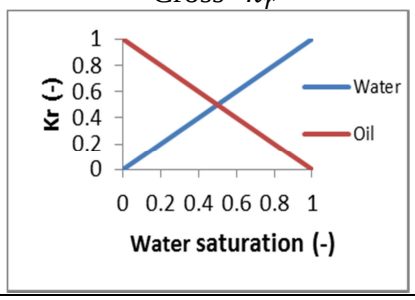
Capillary pressure P_c [bar = 10^4 kgms^{-2}]	Brooks Corey (λ=2) 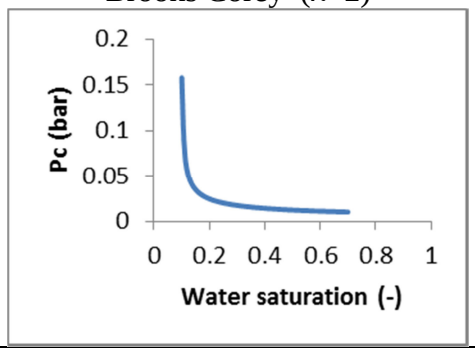	Null capillary pressure

Table 1. Set up of main flow parameters for calculations of two-phase flow in fractured systems depicted in Fig. 7 and 10. The relative permeability and capillary pressure as functions of water saturation in the matrix obey the Brooks and Corey model (1964) with λ (=2) the so-called pore-size distribution index.

	x direction	*y* direction
k_f [10^{-15} m^2]	46.42	120
k^{FN-S} [10^{-15} m^2]	40	120
ϕ^{FN-S} [-]	0.004	0.012
ϕ_f [-]	0.012	

Table 2. Main macroscopic parameters of the fractured block in Fig. 7 to infer via the oriented block size technique the mean matrix block size of a dual porosity model. k_f, ϕ_f respectively are the permeability and porosity of the whole block, k^{FN-S}, ϕ^{FN-S} respectively are the permeability and porosity of the fracture network at the sides (normal to *x* and *y* directions) of the block.

Block sizes	OBS	GI	MS	EGI-large	EGI-small
s_x [m]	0.360	0.6	0.35	0.696	0.257
s_y [m]	0.306	0.3	0.345	0.494	0.257

Table 3. Mean matrix block sizes of a dual porosity model as a surrogate to the discrete fracture network in Fig. 7.

Two different types of flow are simulated, the first one with low water injection rate of 0.1 m/day in the fractures and low matrix permeability of 10^{-15} m^2, the second one with higher injection rate of 1 m/day and higher matrix permeability of 10^{-14} m^2 . On the one hand, the first scenario with small water fluxes in the fractures and weakly permeable matrix enhances capillary effects as the origin of pressure gradients between fracture and matrix and subsequent exchange rates between both media Due to capillary effects in the matrix and absence of these in the fractures, the oil pressure in the matrix is higher than that in the fractures and oil is ejected from the matrix (or water invades the matrix). On the other hand, the second scenario with high injection velocities favors "piston" flow in the fractures and enhances fracture-matrix exchanges as the consequence of the excess of water pressure in fractures compared with oil pressure in the matrix. Water invades the matrix and the process

572 is enhanced by the contrast of mobility (the ratio kr/μ) between oil and water phases which
573 triggers rapid water invasion along the fractures and early leaching of matrix blocks.

574 To reinforce these assertions about flow scenarios with contrast between capillary and
575 viscous forces to extract oil from matrix blocks, we also calculated a dimensionless capillary
576 number based on the evaluation of water fluxes invading matrix blocks versus expulsion of oil
577 from the matrix to fractures by capillary pressure contrasts. With steady-state flow sweeping
578 oil from the system by forced water injection at one side of the fractured block, the mean
579 water pressure gradient in the system is evaluated as

580 $$\left|\nabla P_w\right| \approx \frac{V_{inj}\mu_w}{k_i^f} \quad (15)$$

581 P_w [$ML^{-1}T^{-1}$] is the water pressure in both the fractures and the matrix, V_{inj} [LT^{-1}] is the
582 injection velocity of water at the upstream side of the fractured block, μ_w [$ML^{-1}T^{-1}$] is the
583 dynamic viscosity of water, and k_i^f [L^2] is the equivalent fracture permeability of the whole
584 block along the direction i of water injection. Regarding the capillary pressure gradient, we
585 assume a null capillary pressure in the fractures (open medium of unit porosity) and we take
586 in the matrix the maximal capillary pressure $P_c^{\max}$ given by relationships capillary pressure –
587 saturation (see, e.g., Table 1). The capillary pressure gradient between matrix and fractures is
588 then approximated as

589 $$\left|\nabla P_c\right| \approx \frac{P_c^{\max}}{s_{\min}/2} \quad (16)$$

590 with $s_{\min}$ [L] the smallest dimension (in either directions x, or y or z) of the mean matrix
591 block size. A dimensionless capillary number balancing capillary gradient with water pressure
592 gradient can be expressed as

593 $$n_c = \frac{\left|\nabla P_c\right|}{\left|\nabla P_w\right|} \approx \frac{2P_c^{\max}k_i^f}{s_{\min}\mu_w V_{inj}} \quad (17)$$

This capillary number is larger than one for flow conditions dominated by capillary forces as it becomes close to one or less than one when viscous forces condition flow in the fractured block.

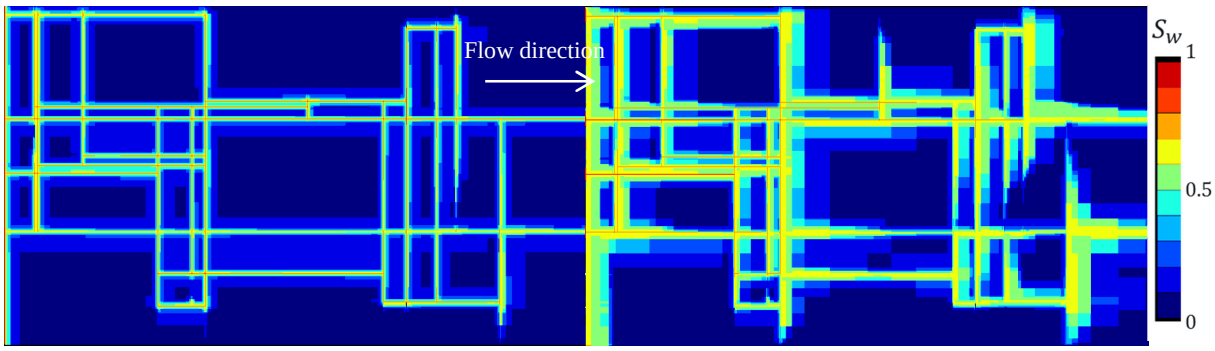

Fig. 8. Maps of water saturation in a water-flooding two-phase flow scenario. Calculations are performed over a fine grid discretizing both the fracture network and matrix (system in Fig. 7). The system is initially saturated in oil and water is injected in the fractures at a constant flow rate at the western boundary of the system. Oil recovery is monitored at the eastern boundary (see Fig. 9). The fluid exchange between fractures and matrix is dominated by capillary forces in map *a* as both capillary and viscous forces are active in map *b*.

In the DFN approach where matrix-fracture exchanges are dominated by capillary effects ($n_c = 4.1$ with the settings of the simulations), water does not deeply invade the matrix (Fig 8.a,) while for the same injected water pore volume, high injection velocity and piston flow ($n_c = 0.41$) maintains higher water pressure gradients that help to a deeper water invasion of the matrix (Fig. 8.b). Calculations in the DFN serve as reference to the comparison of flow scenarios between dual porosity models assigned with matrix block size from the GI, EGI, MS and OBS methods (sizes of blocks are pictured in Fig. 7). The comparison is here performed by way of a single indicator defined as the evolution in time (precisely, the evolution with the water pore volume injected in the system) of the oil recovery ratio at the outlet of the fractured system. This oil recovery corresponds to the ratio of the cumulative volume of oil exiting the system to the total initial volume of oil in the system. This indicator is obviously macroscopic, with the meaning that it monitors the

behavior of the system at the large scale (at least the homogenization scale of the fracture network). It would not make sense to compare a local feature of the fracture network (e.g., the pressure transients in a single fracture) with averaged behaviors obtained for the large blocks (cells) of a dual porosity approach.

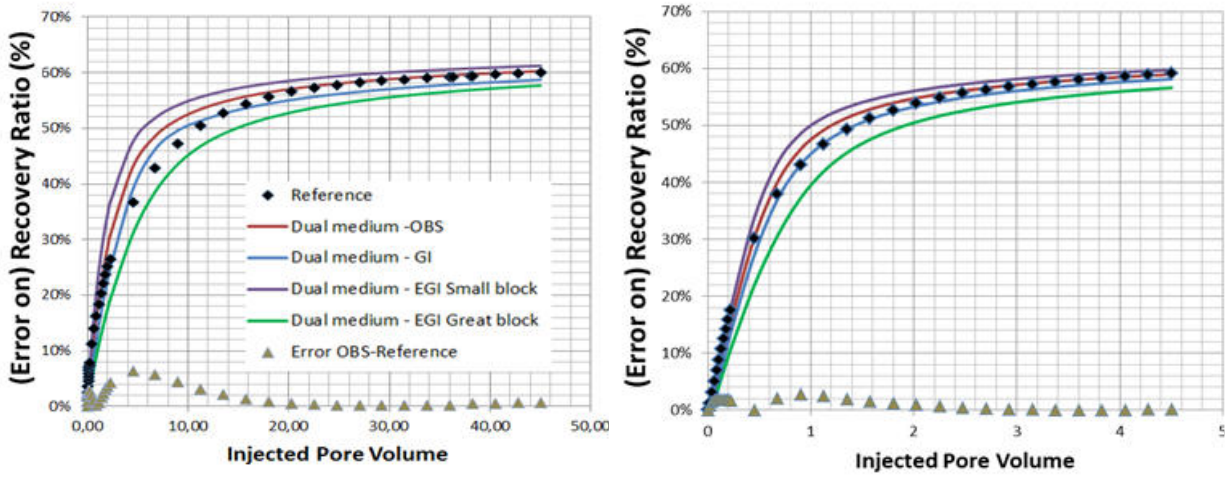

a **b**

Fig. 9. Oil recovery ratio versus water injected pore volumes at the eastern boundary of a fractured network (in Fig. 7). The so-called reference is calculated by means of a finely discretized network as the other curves are drawn from a dual porosity model with various mean matrix block sizes. Results from the mean spacing technique for matrix block size evaluation are not reported because they are merged with those from the oriented block size technique. Capillary forces dominate the exchange rate between fractures and matrix in plot *a*, as both capillary and viscous forces are active in plot *b*.

Fig. 9 presents two plots of the oil recovery ratio as a function of the injected pore volume and stemming from flow scenarios with low and high injection velocities. The same oil recovery ratio of approximately 60% is reached for both flow scenarios, but with only 5 pore volumes in the case of high injection velocity compared with the 50 pore volumes required by the case of low injection velocity. No dual porosity model with their different matrix block size renders results that completely depart from the reference calculations in the DFN. Since matrix block sizes calculated with OBS and MS techniques are quite similar (see

Fig. 7 and Table 3), the results form dual porosity model simulations do not differ significantly and only outputs from the OBS technique are reported in Fig. 9.

The OBS technique tends to slightly underestimate the matrix block size which triggers a quicker oil extraction from the matrix and produces recovery curves slightly shifted toward short injection times. The simulations handling the GI matrix blocks are also in very good agreement with references, especially in the case of fracture-matrix exchanges enhanced by high water injection rate. The matrix block sizes of EGI are still underestimated by the "small block" measure and overestimated by the "large block" measure giving rise to respectively faster and slower evolutions of the oil recovery ratio with respect to time. As such, the EGI technique is not the most accurate to calculate matrix block sizes and should be employed as a convenient way to provide minimal and maximal bounds to these sizes. Notably, the fractured system discussed above does not significantly distinguish between GI and OBS in terms of accuracy whichever the mechanism prevailing in fluid flux exchanges between fractures and matrix. Nevertheless, we are reminded that the reference fracture network was built to mitigate GI downsides. Fracture dead-ends were removed from the network and the two fractures families were set parallel to the x and y directions of the fractured block, thus allowing the GI method to infer a precise "invasion curve" ($A(X)$ in Appendix B). This is why GI shows good performances in the present test cases as it exhibited more discrepancies in the geometrical test cases discussed in Section 3.

At this stage, it must be raised that the OBS technique partly relies upon evaluations of block-side properties such as fracture porosity and permeability, the latter being eventually not representative of inner-block quantities when the portion of fractures intercepting the block sides are not representative of the network geometry inside the block. To address the eventual influence of this downside, we recalculated the two flow scenarios discussed above for another fractured system (Fig. 10) which comprises a few long fractures located very close

to the sides of the system. These fractures delimit a few very elongated matrix blocks close to the boundaries of the system (those encircled in Fig 10) as the majority of matrix blocks inside the system are rectangular with a ratio length to width barely exceeding a factor 3. As expected, the inner-block and block-side properties used by the OBS method (Table 4) differ from that of the fractured "regular" system previously discussed.

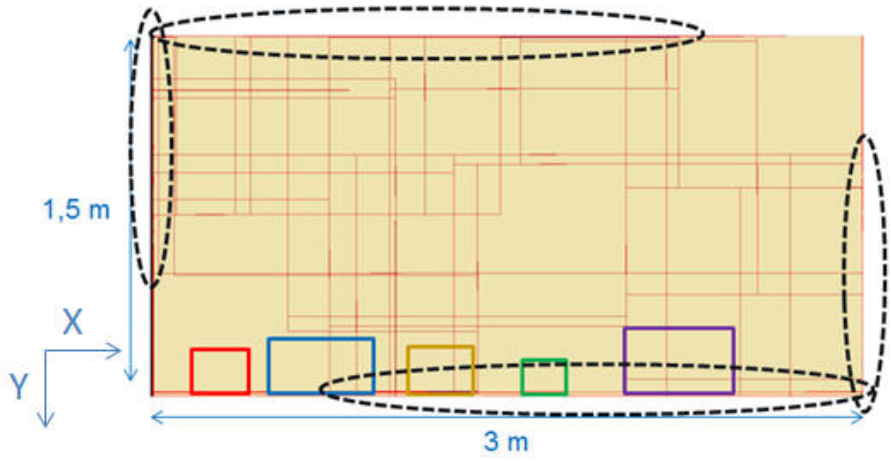

Fig. 10. Two-dimensional fracture network serving as a system finely discretized or handled as a dual-porosity model. Fractures close to the boundaries delimit very narrow matrix blocks (encircled) that depart from the shape of blocks within the fracture network. The identified sizes of matrix blocks in a dual porosity approach are reported as colored frames, from left to right: Red = oriented block size method, Blue = general imbibition method, Orange = mean spacing imbibition method, Green and Purple = small and large sizes from enhanced general imbibition method.

	x direction	*y* direction
k_f [10^{-15} m^2]	107.72	240
k^{FN-S} [10^{-15} m^2]	106.66	240
ϕ^{FN-S} [-]	0.0106	0.024
ϕ_f [-]	0.024	

Table 4. Main macroscopic parameters of the fractured block in Fig. 10 to infer via the oriented block size technique the mean matrix block size of a dual porosity model. k_f, ϕ_f respectively are the permeability and porosity of the whole block, k^{FN-S}, ϕ^{FN-S} respectively are the permeability and porosity of the fracture network at the sides (normal to x and y directions) of the block.

Comparing reference calculations performed over the DFN (maps of water saturation in the system reported in Fig. 11, capillary number n_c of 19 for Fig. 11a and of 1.9 for Fig 11b) and calculations in the dual porosity models reveals that the oil recovery ratio is still of approximately 60% after 4-5 injected pore volumes for high injection velocity and 40 pore volumes under low injection velocity conditions (Fig. 12).

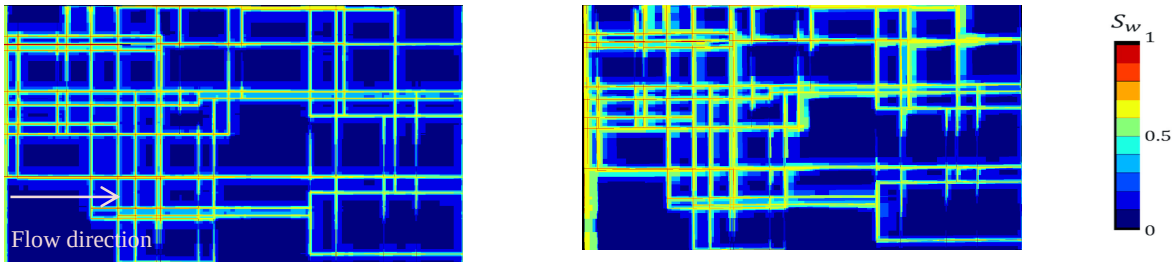

a **b**

Fig. 11. Maps of water saturation in a water-flooding two-phase flow scenario. Calculations are performed over a fine grid discretizing both the fracture network and matrix (system in Fig. 10). The system is initially saturated in oil and water is injected in the fractures at a constant flow rate at the western boundary of the system. Oil recovery is monitored at the eastern boundary (see Fig. 12). The fluid exchange between fractures and matrix is dominated by capillary forces in map a as both capillary and viscous forces are active in map b.

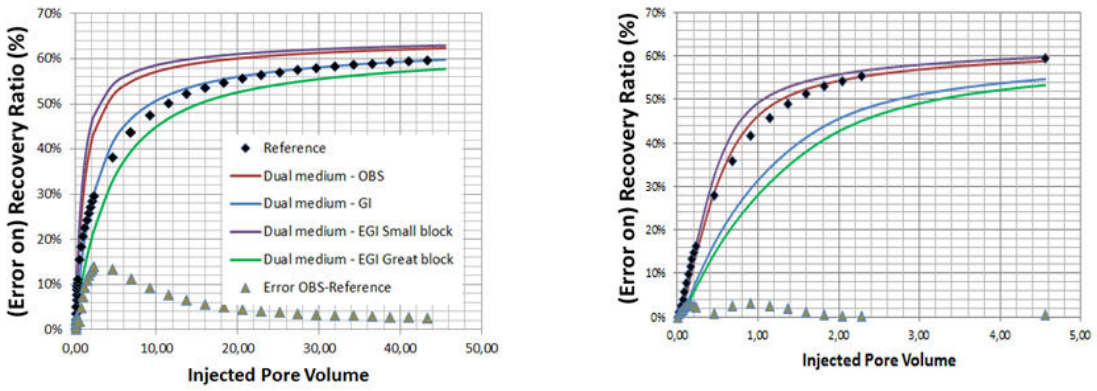

a **b**

Fig. 12. Oil recovery ratio versus water injected pore volumes at the eastern boundary of a fractured network (in Fig. 10). The reference curve is calculated by means of a finely discretized network as the other curves are drawn from a dual porosity model with various mean matrix block sizes. Results from the mean spacing technique are not reported because they are merged with those from the oriented block size technique. Capillary forces dominate the exchange rate between fractures and matrix in plot *a*, as both capillary and viscous forces are active in plot *b*.

693 This result confirms that the macroscopic behaviors of both the DFN and its
694 representation as a dual porosity system are changed much by the few fractures that do not
695 obey the general geometric and structural settings of the whole fractured block. This feature is
696 also evidenced by the comparison between the maps of water saturation in Fig. 8 and Fig. 11
697 that only differ by the locations of fractures underlined by high water saturations. However,
698 discrepancies between the reference (taken as the DFN) and the dual porosity approximations
699 increase. As for the preceding example, OBS and MS techniques provide very similar matrix
700 block sizes (these sizes are pictured in Fig. 10 and reported in Table 5) and similar dual-
701 porosity behaviors making that MS results are not discussed in the following.
702

Block sizes	OBS	GI	MS	EGI-large	EGI-small
s_x [m]	0.185	0.44	0.24	0.47	0.147
s_y [m]	0.149	0.21	0.19	0.325	0.138

703

704 Table 5. Mean matrix block sizes of a dual porosity model as a surrogate to the discrete
705 fracture network in Fig. 7.
706

707 In the case of matrix-fracture exchanges dominated by capillary forces (Figs 11a, 12a)
708 the OBS technique overestimates the leaching of matrix block (and oil production at the
709 outlet of the system) because the smallest matrix block size (here along the *y* direction) is
710 underestimated. Whichever the algebraic form chosen in OBS to infer the matrix block size
711 (See Section 2), the method is in essence sensitive to fracture densities close to the boundaries
712 of the whole fractured block, either in regard of porosities at the sides of the block or of
713 permeability values in a "permeameter" type system. If the actual matrix block sizes close to
714 the boundaries of the block are smaller than inside the block, as is the case with the present
715 example, the smallest matrix block size (here along *y*, see Table 5) is underestimated which

favors rapid imbibition under capillary forces (see above the capillary number n_c) . Notably, the GI technique is not sensitive to the few small matrix blocks of the DFN because it treats the shell and inner parts of the block exactly the same way. For its part, the "small" EGI technique underestimates the mean matrix block size as the "Large" EGI overestimates it ("small" EGI overestimates matrix imbibition and "Large" EGI underestimates imbibition, see oil recovery in Fig. 12a compared with reference).

When matrix-fracture exchanges occur as a conjunction of viscous and capillary forces (see the capillary number in (17) and subsequently evaluated for DFN simulations), the OBS technique renders results the closest to reference. The key is that rapid water invasion of the fractured block through permeable fractures (see Fig. 11b) and subsequent viscous effects between matrix and fractures are dominated by percolation through the large fractures and their (large) neighbor matrix blocks. As the OBS technique identifies the correct largest matrix block size (here along the *x* direction, see Table 5), flow simulations with a dual porosity model are convincing. This time, the GI technique underestimates oil recovery, as "Large" EGI does too, because the overestimated matrix block size (especially along the *x* direction, see Table 5) is favorable to capillary imbibition but hampers water invasion along fractures and matrix block leaching at early injection times.

Finally, regarding performances in terms of computation costs, the different geometric methods were applied to a large DFN represented as a synthetic dual porosity reservoir of 1.05 million grid cells. For OBS and MS methods, matrix block size calculations were performed for each elementary cell and duplicated over all cells of the reservoir with total CPU times coming up as: 230 s for OBS and 1120 s for MS. Notably, the time counted for GI and EGI is that of calculations over a limited number of cells "strategically" sampled in the whole grid of the dual porosity reservoir, yielding a fair representation of the system after 1800 s of calculation. With approximately 4 s of calculation per cell and 10^6 cells, identifying

741 a matrix block size for each cell with GI and EGI methods would render impracticable
742 evaluations exceeding 45 days. When applied to known DFNs, both OBS and MS require a
743 pre-evaluation of the diagonal permeability tensor of the fractured block; by construction for
744 OBS (see Section 2) and to identify main flow directions in MS for which random lines
745 counting the spacing of fractures (see Appendix B) are parallel to these directions.
746 Differences of computations times between methods are in the straightforward (and fast)
747 application of an analytical solution for OBS opposed to the need for many random draws in
748 MS.
749
750 **5. Conclusions**
751 The Oriented Block Size (OBS) technique has been developed as a new way to infer
752 the mean matrix block sizes in porous fractured media with application to dual porosity
753 models of flow at the large scale. Matrix block sizes are calculated by seeking the equivalence
754 in terms of fracture permeability and fracture porosity between a fractured block and a
755 Warren and Root discrete fracture network made of three fracture families with regular
756 spacing and fracture planes normal to the main flow directions.
757 Two expressions of the OBS are available according to which type of fractured block
758 the method is applied. The first expression is well suited to infer matrix block sizes over
759 synthetic discrete fracture networks or well-known actual networks since it requires
760 identifying fracture porosity of the network, fracture porosity at the sides of the fractured
761 block, and the diagonal permeability tensor of the whole block (which can be calculated
762 analytically or numerically). This first expression is based on a rigorous algebraic
763 development which reveals precise and renders matrix block sizes close to expectations drawn
764 from various synthetic discrete fracture networks. The second expression is derived from the
765 first one via assumptions on the fracture porosities of the block. It has the advantage of being

applicable to hardly accessible fracture network as encountered in the field. This second expression is compatible with an inference from field measurements such as hydraulic tests and observations in wells but should only render orders of magnitude instead of pinpoint values. Further works should address how matrix block sizes are influenced by uncertainty on available field data.

The OBS technique revealed much faster in terms of computation times compared with other available geometrical techniques developed to infer matrix block sizes. This feature is a promising avenue for tentative applications of the method in up-scaling the representation of huge fractured reservoirs as done for instance in the oil industry when optimization of oil recovery from various exploitation scenarios is planned. In this context, OBS and its precise evaluation of matrix block sizes is useful to the parameterization of dual porosity models for two phase flow either dominated by capillary forces or viscous forces. However, as the other methods, the OBS technique may fail in retrieving matrix block sizes within poorly connected fracture networks. It is worth to note however that poorly connected networks are not valuable candidates to homogenization into a dual porosity model.

Finally, it must also be raised that OBS is associated with the identification of large scale permeability tensors that are mostly sensitive to the backbone of a fractured network and do not see fracture dead-ends. In the case of applications relying upon data from hydraulic well tests, the type of occurring flow should be carefully considered. Two phase flow, mostly witnessed by the propagation of an oil/water saturation front, will mainly record the effects of the backbone, as single phase flow, mainly monitored by the transient evolution of water pressure heads, would also be sensitive to dead-ends. It deserves some additional synthetic test cases or confrontation to actual field data to see whether or not the OBS technique reveals suited in these instances.

Acknowledgments

The authors are grateful to IFPEN for funding the Ph-D fellowship of C. Jerbi. They are also indebted to P. Delaplace at IFPEN for its fruitful advices provided all along this study.

Appendix A. Matrix block sizes extracted from the equivalence between an actual fractured block and a Warren and Root (WR) block.

We remind that an actual and well connected fractured block oriented with its main directions along the main directions of flow indexed by *i*=1,2,3, can be characterized by mean permeabilities k_i^{FN-S} along the sides of the block as

$$k_i^{FN-S} = \frac{1}{2\left(\Delta_{i+1}\Delta_{i+2}\right)}\left(\sum_{n=1}^{Nf_{i-}} k_n l_n e_n + \sum_{n=1}^{Nf_{i+}} k_n l_n e_n\right) \quad \text{(A1)}$$

The block size in direction *i* is denoted Δ_i and the sides delimiting the block are also indexed by *i* but for limits normal to the main direction *i*. In addition, block sides are labelled $i-$ or $i+$ according to their respective location upstream or downstream along direction *i*. In (A1), *i* is a cycling index such that, e.g., *i*+1 = 3 when *i* = 2 and *i*+1 returns to 1 when *i*=3. The sides $i-$ and $i+$ of the block are intercepted by a number of fractures Nf_{i-} and Nf_{i+}, and *k* is the local permeability of a fracture intercepting the side of the block over an apparent length *l* and with apparent fracture aperture *e*.

We also remind that a Warren and Root (WR) block concealing a regular fracture network of three fracture families can be characterized by two expressions associating: 1- the diagonal tensor of permeability of the whole block $k_i^{WR}(i=1,2,3)$, 2- the mean porosity of the block ϕ^{WR}, and 3- the porosity of the block sides $\phi_i^{WR-S}(i=1,2,3)$, with the spacing $s_i(i=1,2,3)$, the aperture $e_i(i=1,2,3)$, and the local permeability $k_i(i=1,2,3)$ of the three fracture families composing the WR block (for details, see Section 2). These expressions are

$$k_i = \frac{1}{2}\left(1+\frac{s_i}{e_i}\right)\sum_{j=1}^{3}(-1)^{\delta_{i,j}} k_j^{WR} \quad \text{(A2)}$$

$$k_i = \frac{1}{2\left(\phi^{WR}-\phi_i^{WR-S}\right)}\sum_{j=1}^{3}(-1)^{\delta_{i,j}} k_j^{WR} \quad \text{(A3)}$$

where $\delta_{i,j}$ is the Kronecker symbol, $\delta_{i,j}=1, i=j; \delta_{i,j}=0, i\neq j$.

Following the idea that one can establish the equivalence between a WR network and an actual fractured block regarding their hydraulic properties, it is assumed that ϕ^{WR}, ϕ_i^{WR-S}, and k_i^{WR} are similar to the equivalent properties in the actual fractured block, respectively denoted as ϕ^{FN}, ϕ_i^{FN-S}, and k_i^{FN-S} (see A1, for the latter). In the same vein, if a WR network serves as reference for fixing model parameters of homogenized approaches to fractured media, the characteristics of a WR network can be substituted by parameters of the homogenized model. For example, the characteristics s_i, e_i, and k_j^{WR} in (A2) are respectively substituted by a mean matrix block size (also denoted s_i as defined in (3)), a mean fracture aperture e_f, and the entries of a diagonal tensor $\mathbf{k}_j^f$ of the homogenized model. With these transformations, equating (A2) and (A3) results in

$$\left(1+\frac{s_i}{e_f}\right)\sum_{j=1}^{3}(-1)^{\delta_{i,j}}k_j^f=\frac{1}{\left(\phi^{FN}-\phi_i^{FN-S}\right)}\sum_{j=1}^{3}(-1)^{\delta_{i,j}}k_j^{FN-S}\ ;\ i.e.,$$

$$s_i=e_f\left(\frac{\sum_{j=1}^{3}(-1)^{\delta_{i,j}}k_j^{FN-S}}{\left(\phi^{FN}-\phi_i^{FN-S}\right)\sum_{j=1}^{3}(-1)^{\delta_{i,j}}k_j^f}-1\right) \qquad \text{(A4)}$$

For the sake of simplification (see hereafter), the term -1 in the expression of s_i can be dropped by considering that the term in $(\phi^{FN})^{-1}$ is much larger than one for usual fracture porosity of a rock block barely exceeding a few percent. Stated differently, one might also consider in (A4) that the matrix block size s_i is much larger than the fracture aperture e_f and results in

$$s_i\approx e_f\frac{\sum_{j=1}^{3}(-1)^{\delta_{i,j}}k_j^{FN-S}}{\left(\phi^{FN}-\phi_i^{FN-S}\right)\sum_{j=1}^{3}(-1)^{\delta_{i,j}}k_j^f} \qquad \text{(A5)}$$

The mean matrix block size s_i in (A5) depends on both the mean fracture aperture e_f and the fracture permeability of a homogenized model k_j^f. It is noteworthy that e_f is usually not a parameter of a homogenized approach, and it makes sense to render (A5) (partly) independent of any conjecture on the value of e_f. To this end, it is reasonably assumed that a WR network has its matrix block sizes separating neighbor fractures independent of the apertures e_i of the fractures. Stated differently, it is assumed that a WR network with a uniform aperture e_f for its three fracture families can be found as equivalent to a WR with its three fracture families with apertures e_i. With a uniform aperture e_f, a WR network would render a value $\phi^{WR} - \phi_i^{WR-S} = e_f Nf_i / \Delta_i$ with Nf_i the number of fractures in the family *i*, and Δ_i the size of the whole fractured block along direction *i*. If the values $\phi^{FN} - \phi_i^{FN-S}$ were not replacing their equivalent $\phi^{WR} - \phi_i^{WR-S}$ in Eq (A5), the latter would no longer depend on e_f. Hence, our proposal is to calculate porosities of the actual fracture network by assigning the whole skeleton of the network with a constant single-fracture aperture e_f. The fracture network porosities for a constant aperture e_f would write as

$$\left(\phi^{FN} - \phi_i^{FN-S}\right)\Big|_{e=e_f} = e_f \left(\phi^{FN*} - \phi_i^{FN-S*}\right) \tag{A6}$$

The terms ϕ^{FN*}, ϕ_i^{FN-S*} [L^{-1}] denote porosities of the actual fracture skeleton per unit fracture aperture (that can be calculated by assigning a uniform fracture aperture of 1 to the whole fracture network). Substituting (A6) in (A5) simplifies the formulation of the matrix block size into

$$s_i \approx \frac{\sum_{j=1}^{3} (-1)^{\delta_{i,j}} k_j^{FN-S}}{\left(\phi^{FN*} - \phi_i^{FN-S*}\right) \sum_{j=1}^{3} (-1)^{\delta_{i,j}} k_j^{f}} \tag{A7}$$

The main characteristic of (A7) is that the mean matrix block size depends: 1- on a mean permeability tensor k_j^f of fractures at the scale of a (mesh of a) homogenized model of the system (e.g., a conjecture of the fracture permeability in a dual porosity model), 2- on the facet permeability values of the actual fracture network k_j^{FN-S}, and 3- on structural properties of the actual network resulting in fracture porosity values of the whole fractured block and its sides ϕ^{FN*} and ϕ_i^{FN-S*}, respectively. These features make that the form in (A7) is hardly applicable to poorly-known natural systems and should be mainly used in problems dealing with homogenization of systems with well-known geometry and discretization of synthetic fracture networks and matrix blocks.

Nevertheless, another form of the mean matrix block size can be proposed. By manipulating (A1), the permeability of the actual fracture network at the facets of the whole fractured block can be rewritten as

$$k_i^{FN-S} = \frac{\left(\sum_{n=1}^{Nf_{i-}} l_n e_n + \sum_{n=1}^{Nf_{i+}} l_n e_n\right)}{2\left(\Delta_{i+1}\Delta_{i+2}\right)} \times \frac{\left(\sum_{n=1}^{Nf_{i-}} k_n l_n e_n + \sum_{n=1}^{Nf_{i+}} k_n l_n e_n\right)}{\left(\sum_{n=1}^{Nf_{i-}} l_n e_n + \sum_{n=1}^{Nf_{i+}} l_n e_n\right)} \;;\; i.e.,$$

$$k_i^{FN-S} = \phi_i^{FN-S}\overline{k_i} \quad with \quad \overline{k_i} = \frac{\left(\sum_{n=1}^{Nf_{i-}} k_n l_n e_n + \sum_{n=1}^{Nf_{i+}} k_n l_n e_n\right)}{\left(\sum_{n=1}^{Nf_{i-}} l_n e_n + \sum_{n=1}^{Nf_{i+}} l_n e_n\right)} \tag{A8}$$

The tensor components $\overline{k_i}$ (i=1,2,3) in (A8) are an arithmetic mean of single-fracture permeability values weighted by open fracture surface areas at the sides of the whole fractured block. If we assume that these mean values are equal, irrespective of the facet of the fractured block (which also can go with fractured systems candidates to homogenization), it also means that the eventual anisotropy of permeability in the fracture network is just the consequence of fractures densities normal to the flow directions, i.e., $k_i^{FN-S} = \phi_i^{FN-S}\overline{k}$. Notably, this strong assumption stating that one can define a constant single-fracture

permeability value $\overline{k}$ also goes with the existence of an equivalent uniform single-fracture aperture e_f for the whole fracture network. Reintroducing in (A5) the expression (A8) with a constant value $\overline{k}$ and making use of rescaled porosities defined in (A6) as $\phi_i^{FN-S} = e_f \phi_i^{FN-S*}$ comes down to

$$s_i \approx \frac{e_f \overline{k} \sum_{j=1}^{3} (-1)^{\delta_{i,j}} \phi_j^{FN-S*}}{\left(\phi^{FN*} - \phi_i^{FN-S*}\right) \sum_{j=1}^{3} (-1)^{\delta_{i,j}} k_j^f} \tag{A9}$$

It can also be shown that a WR network with constant aperture e_f for its three fracture families has block and side porosities following the relation $\sum_i \phi_i^{WR-S*} = 2\phi^{WR*}$. If the rescaled DFN is equivalent to the WR network, then one can state that $\sum_i \phi_i^{FN-S*} = 2\phi^{FN*}$. Noting that $\sum_{j=1}^{3} (-1)^{\delta_{i,j}} \phi_j^{FN-S*}$ can also be rewritten as $\sum_{j=1}^{3} \phi_j^{FN-S*} - 2\phi_i^{FN-S*}$ and reintroducing the preceding relationship between block and side porosities in (A9) results in

$$s_i \approx \frac{2 e_f \overline{k}}{\sum_{j=1}^{3} (-1)^{\delta_{i,j}} k_j^f} \tag{A10}$$

In the case of field applications with poorly known and hardly accessible fracture networks, (A10) returns the mean matrix block sizes in a fracture network based on the field evaluations of the permeability tensor $\mathbf{k}^f$ of a whole fractured block, the average uniform aperture e_f and permeability $\overline{k}$ of a single fracture. Because the entries of (A10) are not straightforward to obtain and may also be associated with important measurement errors, it is expected that (A10) will only render orders of magnitude of mean matrix block sizes.

Appendix B. Structural-geometrical evaluations of a mean matrix block size in a dual continuum flow model

The geometrical imbibition (GI) method

The method has been developed for two-dimensional flow models only. Three-dimensional approaches are therefore handled as multilayer systems. For a two-dimensional image of an actual or synthetic fracture network, the first task to handle consists in mapping the image on a regular grid of square pixels. Each pixel is then assigned a value d_f that represents the distance between the center of the pixel and the closest fracture of the network. One sums up the area of pixels whose distance d_f is less than a prescribed value X, and the area is then normalized by the total surface area of the image to form the quantity $A(X)$. The resulting measure $A(X)$ (Fig. B1) is modeled as

$$A(X) = \frac{2X}{a} + \frac{2X}{b} - \frac{4X^2}{ab} \qquad \text{(B1)}$$

with a and b the resulting mean size of the matrix block of a two-dimensional dual porosity model. a and b are obtained by minimizing the sum of squared errors between the model in (B1) and the actual measures of $A(X)$.

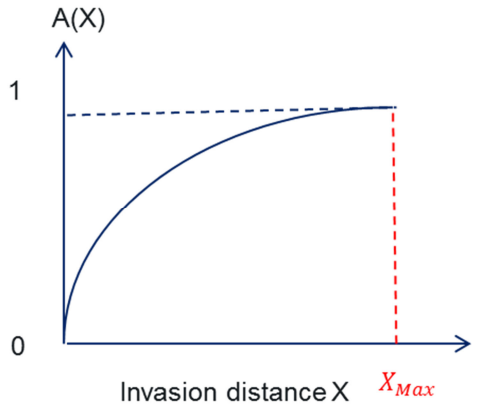

Fig. B1. General imbibition technique to mean matrix block size identification. Normalized invaded matrix area $A(X)$ as a function of the distance X between a location in the matrix and the closest fracture.

The extended geometrical imbibition (EGI) method

This method improves the two-dimensional GI technique by assuming that two mean matrix block sizes characterize the relationships between fractures and matrix. For locations in the matrix close to fractures, two types of matrix block interact with fractures, whereas locations far from fractures are influenced by a single size of matrix block. This feature makes that the quantity $A(X)$ drawn from the mapping of the actual fracture network (see above the GI technique) is modeled by a discontinuous curve in the form

$$\begin{aligned} A(X) &= \alpha_1\left(\frac{2X}{a_1}+\frac{2X}{b_1}-\frac{4X^2}{a_1b_1}\right)+\alpha_2\left(\frac{2X}{a_2}+\frac{2X}{b_2}-\frac{4X^2}{a_2b_2}\right) \;\; ; \; X \le \frac{a_1}{2} \\ A(X) &= \alpha_2\left(\frac{2X}{a_2}+\frac{2X}{b_2}-\frac{4X^2}{a_2b_2}\right) \;\; ; \; X > \frac{a_1}{2} \end{aligned} \qquad \text{(B2)}$$

with (a_1,b_1), (a_2,b_2) the size of the small and large matrix blocks respectively. α_1,α_2 are the proportions of small (type 1) blocks and large (type 2) blocks with $\alpha_2 = 1-\alpha_1$. The distance $X = a_1/2$ is the threshold beyond which a single type of large matrix block is sufficient to model interactions between fractures and matrix.

The inference of a single set of parameters $(\alpha_1,a_1,b_1,\alpha_2,a_2,b_2)$ by minimizing errors between the model in (B2) and actual measures of $A(X)$ is not straightforward because the subsets of parameters (α_1,a_1,b_1) and (α_2,a_2,b_2) are partly interchangeable to shape the same function $A(X)$. It is better suited to analyze the derivative $A'(X)$

$$\begin{aligned} A'(X) &= \frac{dA(X)}{dX} = \alpha_1\left(\frac{2}{a_1}+\frac{2}{b_1}-\frac{8X}{a_1b_1}\right)+\alpha_2\left(\frac{2}{a_2}+\frac{2}{b_2}-\frac{8X}{a_2b_2}\right) \;\; ; \; X \le \frac{a_1}{2} \\ A'(X) &= \frac{dA(X)}{dX} = \alpha_2\left(\frac{2}{a_2}+\frac{2}{b_2}-\frac{8X}{a_2b_2}\right) \;\; ; \; X > \frac{a_1}{2} \end{aligned} \qquad \text{(B3)}$$

This derivative appears as a decreasing piece-wise linear function of *X* which can be fitted by hand or numerically on the plot of actual values $A'(X)$ (see Fig B2). The parameter a_1 is set

931 so that the break point of the model $A'(X)$ located in $a_1/2$ matches with the change of slope
932 of actual data. The parameter a_2 is defined as the length (distance) for which $A'(a_2/2)=0$
933 (see Fig. B2).

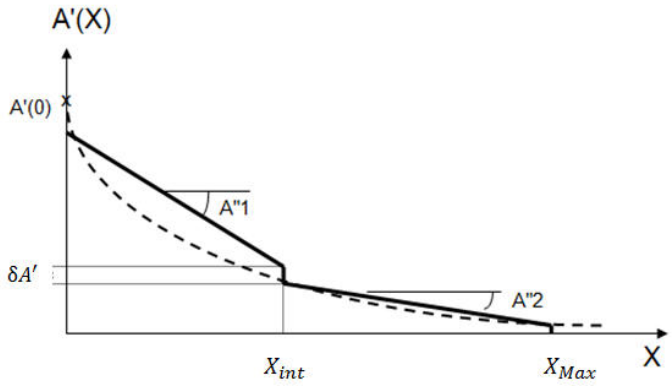

934

935 Fig. B2. Enhanced general imbibition technique to mean matrix block size evaluation. First-order
936 derivative of the normalized invaded matrix area $A(X)$ as a function of the distance X between a
937 location in the matrix and the closest fracture. The derivative with respect to X is modelled as a piece-
938 wise linear function allowing to infer a small and a large matrix block size.

939

940 The threshold $a_1/2$ separates the linear function $A'(X)$ in two portions with slopes

941
$$A"_1=\frac{dA'(X)}{dX}=-\frac{8\alpha_1}{a_1b_1}-\frac{8\alpha_2}{a_2b_2}\ ;\ X\le\frac{a_1}{2}$$
$$A"_2=\frac{dA'(X)}{dX}=-\frac{8\alpha_2}{a_2b_2}\ ;\ X>\frac{a_1}{2} \qquad \text{(B4)}$$

942 The difference of slopes on a plot of $A'(X)$ can be identified with the expression of
943 $A"_1-A"_2=-8\alpha_1/a_1b_1$ which in turn fixes the ratio α_1/b_1 since a_1 has been previously
944 prescribed.

945 The height of the step between the two linear portions of $A'(X)$ can be calculated as

946
$$\delta A'=A'\left((a_1/2)^-\right)-A'\left((a_1/2)^+\right)=\frac{2}{\alpha_1}\left(\frac{1}{a_1}-\frac{1}{b_1}\right) \qquad \text{(B5)}$$

Identifying (B5) with the value of the plot and associating the result with the identified value $A''_1(X) - A''_2(X)$ renders two equations allowing for the calculation of both α_1 and b_1 values.

Finally, the expression of $A'(X)$ in $X = 0$ which writes as

$$A'(0) = \alpha_1\left(\frac{2}{a_1} + \frac{2}{b_1}\right) + (1-\alpha_1)\left(\frac{2}{a_2} + \frac{2}{b_2}\right) \quad \text{(B6)}$$

is identified via the equivalent value observed on the plot of actual data (Fig. B2) and returns the value of b_2.

The mean spacing (MS) technique

The principle of MS is sketched in Fig. B3.

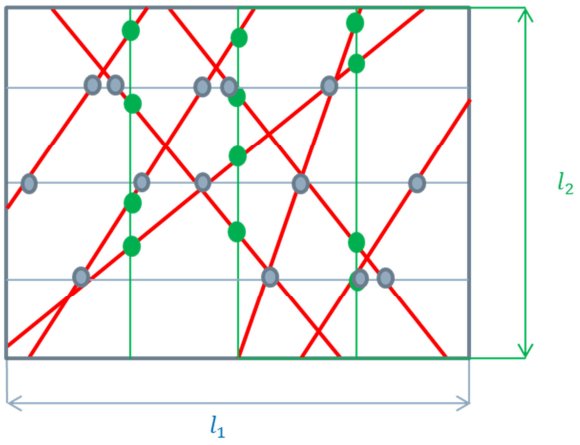

Fig. B3. Mean spacing technique to mean matrix block size evaluation. Distances between neighbor fractures are measured via the intersections between the fracture network and random lines parallel to the main directions of the fractured block.

For each main direction *i* of a fractured block with length l_i, random lines parallel to direction *i* and crossing the whole block are drawn. For each line, one counts as n_i the number of intersections between the line and any fracture plane (or trace in a two-dimensional problem) of the fracture network. For each random line in the direction *i*, the mean distance

between two successive intersections is $l_i/(n_i+1)$. The mean size of the matrix block in the direction *i* is defined as

$$s_i = l_i \left\langle \frac{1}{n_i+1} \right\rangle \tag{B7}$$

where averaging $\langle\ \rangle$ is conducted over the whole set of random lines in the direction *i*.

References

Adler, P.M., Mourzenko, V.V., Thovert, J-F., Bogdanov, I., 2005. Study of single and multiphase flow in fractured porous media, using a percolation approach, Dynamics of Fluids and Transport in Fractured Rocks, Geoph. Monog. Series, 162, 33-41.

Acuna, J.A., Yortsos, Y.C., 1995. Application of fractal geometry to the study of networks of fractures and their pressure transient. Water Resour. Res. 31(3), 527-540.

Arbogast,T., 1990. Derivation of the double-porosity model of single-phase flow via homogenization theory. SIAM J. Math. Anal. 21, 823-836.

Barenblatt, G., Zheltov, I., Kochina, I., 1960. Basic concepts in the theory of seepage of homogeneous liquids in fissured rocks. J. Appl. Math. 24, 1286-1303.

Bourbiaux, B., Cacas, M., Sarda, S., Sabathier, J., 1997. A fast and efficient methodology to convert fractured reservoir images into a dual-porosity model. SPE-38907-MS.

Bourbiaux, B., Fourno, A., Delaplace, P., 2006. Method of modelling a porous geological environment through which a network of fractures run. Patent 2,009,098,366.

Bourbiaux, B., 2010. Fractured reservoir simulation: a challenging and rewarding issue. Oil Gas Sci. Technol. 65, 227-238.

Brooks, R.H., Corey, A.T., 1964. Hydraulic properties of porous media: Hydrology papers, Colorado State University. 3.

Coats, K.H., 1989. Implicit compositional simulation of single-porosity and dual porosity reservoirs. SPE -18427-MS.

De Dreuzy, J. R., Rapaport, A., Babey, T., Harmand, J. , 2013. Influence of porosity structures on mixing-induced reactivity at chemical equilibrium in mobile/immobile Multi-Rate Mass Transfer (MRMT) and Multiple INteracting Continua (MINC) models. Water Resour. Res. 49(12), 8511-8530.

Folch, R., Casademunt, J., Hernandez-Machado, A., Ramirez-Piscina, L., 1999. Phase-Field model for Hele Shaw flows in arbitrary viscosity contrasts. I- Theoretical approach. Phys. Rev. E 60(2), 1724-1733.

Fourno, A, Grenier, C., Benabderrahmane, H., Delay, F., 2013. A continuum voxel approach to model flow in 3D fault networks: A new way to obtain up-scaled hydraulic conductivity tensors of grid cells. J. Hydrol. 493, 68-80.

Jourdain, X., Colliat, J.B., De Sa, C., Benboudjema, F., Gatuingt, F., 2014. Upscaling permeability for fractured concrete: meso–macro numerical approach coupled to strong discontinuities. Int. J. Numer. Anal. Met. 38(5), 536-550.

Karimi-Fard, M., Gong, B., Durlofsky, L.J., 2006. Generation of coarse-scale continuous flow models from detailed fracture characterization. Water Resour. Res. 42, W10423.

Kazemi, H., Merrill, L.S., Porterfield, K.L., Zeman, P.R., 1976. Numerical simulation of water-oil flow in naturally fractured reservoirs. SPE Reserv. Eval. Eng. 11(4), 750-758.

Landereau, P., Noetinger, B., Quintard, M., 2001. Quasi-steady two-equation models for diffusive transport in fractured porous media large-scale properties for densely fractured systems. Adv. Water Resour. 24(8), 863-876.

Lemonnier, P., Bourbiaux, B., 2010a. Simulation of naturally fractured reservoirs. State of the art, part 1, Phyiscal mechanisms and simulator formulation. Oil Gas Sci.Technol. 65(2), 239-262.

Lemonnier, P., Bourbiaux, B., 2010b. Simulation of naturally fractured reservoirs. State of the art, part 2, Matrix-fracture transfers and typical features of numerical studies. Oil Gas Sci. Technol. 65(2), 263-286.

Lim, K.T., Aziz, K., 1995. Matrix-fracture transfer shape factors for dual porosity simulators. J. Petrol. Sci. Eng. 13, 169-178.

Long, J.C.S., Remer, J.S., Wilson, C.R., Witherspoon, P.A., 1982. Porous medium equivalent for networks of discontinuous fractures. Water Resour. Res. 18(13), 645-658.

Matthai, S.K., Nick, H.M., 2009. Upscaling two-phase flow in naturally fractured reservoirs. The AAPG Bull. 93(11), 1621-1632.

Narr, W., 1996. Estimating average fracture spacing in subsurface rock. The AAPG Bull. 80(10), 1565-1586.

Neuman, S.P., 1988. A proposed conceptual framework and methodology for investigating flow and transport in Swedish crystalline rock. SKB Swedish Nuclear Fuel and Waste Management Co., Stockholm, September, Arbetsrapport.

Noetinger, B., Estébenet, T., 2000. Up-scaling double porosity fractured media using contineous-time random walks method. Transport Porous Med. 39(13), 315-337.

Noetinger B., Estebenet, T., Landereau, P., 2001. A direct determination of the transient exchange term of fractured media using a continuous time random walk method. Transport Porous Med. 44, 539-557.

Noetinger, B., Jarrige, N., 2012. A quasi steady state method for solving transient Darcy flow in complex 3D fractured networks. J. Comput. Phys. 231, 23-38.

Oda, M., 1985. Geologic analysis of naturally fractured reservoirs. Geotechnique. 35, 483-495.

Park, C.M., Homsy, G.M., 1984. Two-phase displacement in Hele Shaw cells. Theory. J. Fluid Mech. 139, 291-398.

Pruess, K., Narasimhan, T.N., 1985. A practical method for modeling fluid and heat flow in fractured porous media. SPE J. 25(1), 14-26.

Pruess, K. Wang, J.S.Y., Tsang, Y.W., 1990. On thermohydrologic conditions near high-level nuclear wastes emplaced in partially saturated fractured tuff. 2- Effective continuum approximation. Water Resour. Res. 26(6), 1249-1261.

Quintard, M., Whitaker, S., 1993. One and two-equation models for transient diffusion processes in two-phase systems. Adv. Heat Transf. 23, 369-465.

Quintard, M., Whitaker, S., 1996. Transport in chemically and mechanically heterogeneous porous media. Adv. Water Resour. 19, 29-60.

Tatomir, A.B., Szykiewicz, A., Class, H., Helming, R., 2011. Modeling two phase flow in large scale fractured porous media with an extended multiple interacting continua. CMES 77(2), 81-112.

Thomas, L.K., Dixon, T.N., Pierson, R.G., 1983. Fractured reservoir simulation. SPE J. 23(11), 42-54.

Ueda, Y., Murata, S., Watanabe, Y., Funats, K., 1989. Investigation of the shape factor used in the dual-porosity reservoir simulator. SPE-19469-MS.

Unsal, E., Matthäi, S.K., Blunt, M.J., 2010. Simulation of multiphase flow in fractured reservoirs using a fracture-only model with transfer functions. Comput. Geosci. 14, 527-538.

1092 Warren, J.E., Root, P.J., 1963. The behavior of naturally fractured reservoirs. SPE J. 3, 245-
1093 255.